

ABSTRACT

Title of Dissertation: FAILURE MECHANISMS OF PEDIATRIC GROWING ROD CONSTRUCTS

Genevieve A-L. Hill, Doctor of Philosophy,
2017

Dissertation directed by: Fischell Family Distinguished Professor & Department Chair, John P. Fisher, Ph.D., Fischell Department of Bioengineering Research Biomedical Engineer, Maureen L. Dreher, Ph.D., U.S. Food and Drug Administration

Early onset scoliosis (EOS) affects a vulnerable population of young children, and occurs at critical ages when the spine and thorax are developing. Children suffering with EOS have higher mortality rates due to cardiopulmonary complications; therefore, treatment for these patients can be life-saving. Pediatric growing rod constructs are an important treatment option for young patients with severe and progressive spinal deformities because they encourage growth and correction of the spinal curvature through successive lengthening procedures. However, growing rod constructs suffer from complication rates as high as 72%, which often lead to unplanned reoperations. To help prevent future failures of the same root cause, the failure mode and mechanism must be identified, which tell us how and why the

devices failed respectively. This research included the first study to examine multiple, retrieved pediatric growing rod constructs from various sites to systematically investigate these significant items. The retrieval study revealed that rod fracture (failure mode) was due to bending fatigue (failure mechanism), and stress concentrations play an important role in rod fractures. The information obtained from the retrieval study enhanced the understanding of *in vivo* loading conditions experienced by the device and established clinically-relevant parameters for a mechanical bench model. This research also included the development and validation of a novel mechanical bench model that successfully replicated rod fracture due to bending fatigue. A mechanical bench model that is predicated on clinical outcomes can serve as a tool for engineers and researchers who are looking to improve pediatric growing rod constructs as it will enable them to make relevant predictions about the device's resistance to failure. For example, the model was used in this research to investigate how the unique characteristics of pediatric growing rod constructs such as construct configuration and lengthening affect mechanical performance of the device. Key recommendations regarding surgical technique were identified in the retrieval study and verified through bench testing. The data obtained during this research can ultimately be used to reduce failure rates and unplanned revisions in this patient population.

FAILURE MECHANISMS OF PEDIATRIC GROWING ROD CONSTRUCTS

by

Genevieve A-L. Hill

Dissertation submitted to the Faculty of the Graduate School of the
University of Maryland, College Park, in partial fulfillment
of the requirements for the degree of
Doctor of Philosophy
2017

Advisory Committee:
John P. Fisher, Ph.D., Chair
Maureen L. Dreher, Ph.D., Co-Chair
Srinidhi Nagaraja, Ph.D.
Ian M. White, Ph.D.
Aristos Christou, Ph.D.

© Copyright by
Genevieve A-L. Hill
2017

Dedication

I dedicate this dissertation to my husband, family, friends, FDA family, and collaborators. I am touched and honored to have had your support throughout this journey. I completed this dissertation in loving memory of my paternal grandmother, who never defended her doctoral work.

I would also like to dedicate this to the patients and families that donated their implants to help further research for all of those suffering with spinal deformities.

Acknowledgements

This research has been a true testament of collaboration so there are a number of acknowledgments. My research advisors, Maureen Dreher and Srinidhi Nagaraja, have supported my ideas from the beginning and truly helped refine this research into something great. I cannot thank them enough for guiding me to this point! I am forever grateful for the opportunity granted to me by the past and present management within FDA. I must personally thank Ronald Jean, Jon Casamento, Larry Grossman, Anton Dmitriev, Steve Pollack, Mark Melkerson, Barbara Buch, Vincent Devlin, and Christy Foreman. I sincerely appreciate how open-minded the Bioengineering Department at UMD has been and I would like to thank Adam Hsieh, William Bentley, Peter Kofinas, and John Fisher.

The entire Growing Spine Foundation has been fantastic and the main reason the retrieval study was executed successfully. Therefore, I send many thanks to Jeff Pawelek, Behrooz Akbarnia, Paul Sponseller, John Emans, Peter Sturm, the clinical site coordinators (Alexa Greenler, Lindsay Schultz, Craig Remenapp, Michael Troy, and Dong Tran), GSF's Executive Committee, and all of those working tirelessly behind-the-scenes. The bench testing was possible because of the collaboration with Depuy-Synthes Spine and I appreciate Hassan Serhan and Sharon Starowitz for their support. I would also like to acknowledge the following people for their scientific discussions, contributions, and efforts: Renee Adkins, Joshua Cockrum, Austin Bridges, Franklin Tarke, Pablo Bonangelino, Alexia Haralambous, Katherine Kavlock, Erick Gutierrez, Jonathan Peck, Matthew Di Prima, Shiril Sivan, Robert Campbell, Brian Snyder, and Tricia St. Hillaire.

Table of Contents

Dedication	ii
Acknowledgements	iii
Table of Contents	iv
List of Tables	v
List of Figures	vi
List of Abbreviations	x
Chapter 1: Introduction of Scoliosis and Pediatric Growing Rod Constructs	1
Chapter 2: Identification of the Failure Mechanism of Pediatric Growing Rod Constructs	15
Chapter 3: Bench Model Development and Validation	48
Chapter 4: Investigation of Growing Rod Construct Complexity using the Mechanical Bench Model	65
Chapter 5: Investigation of Growing Rod Lengthening using the Mechanical Bench Model	84
Chapter 6: Summary and Future Work	99
Appendices	106
Bibliography	107

List of Tables

Table 1: Patient Characteristics and Demographics of Growing Rod Patients in the Retrieval Cohort vs. Registry.....	20
Table 2: Patient Characteristics and Demographics at Pre-Operative Time Point of Failed vs. Intact Retrieval Groups- Per Patient Analysis.....	26
Table 3: Change in Patient Characteristics and Demographics from Post-Index to Retrieval Time Points of Failed vs. Intact Retrieval Groups	29
Table 4: Rod Diameters and Materials in Failed and Intact Retrieval Groups	30
Table 5: Radiographic Similarities of Failed Constructs Based on Location of Rod Fracture	38
Table 6: Comparison of a titanium alloy retrieval to a titanium alloy in vitro sample to demonstrate validation of the mechanical bench model. Both spinal rods show crack initiation at a stress concentration and surface topography consistent with bending fatigue.....	57
Table 7: Photographs of the six construct configurations. The top row displays the constructs without crosslinks: No Connectors- Rods Only, Side-by-Side Connectors, 40 mm Tandem Connectors, and 80 mm Tandem Connectors. The bottom row displays the constructs with crosslinks: Side-by-Side Connectors Plus 4 Crosslinks, and 80 mm Tandem Connectors Plus 4 Crosslinks. All construct configurations have an active length of 200mm and the axial connectors are placed in the center of the construct (note: constructs with side-by-side connectors have offset pedicle screws in the superior test blocks). Fixtures include steel U-frames with pins attached to UHMWPE test blocks with the load cell on the bottom.....	69
Table 8: Results of Static Compression Bending Tests. Means in each column that do not share a letter, symbol, or number are significantly different.	74
Table 9: Construct Groups	91
Table 10: Results of Static Compression Bending Tests for Phase I Study.	93

List of Figures

Figure 1: Measurement of Cobb angle on X-ray. Two lines (solid blue) are drawn parallel to the vertebrae at each end of a spinal curve. Two additional lines (dashed pink) are drawn perpendicular from the solid blue lines. The Cobb angle (white arc) is the angle at which the perpendicular lines (dashed pink) intersect. 3

Figure 2: Types of implant components in growing rod constructs. Left: X-ray of a dual growing rod construct with spine-based fixation, tandem axial connector, and two optional crosslinks. Right: X-ray of a dual growing rod construct with rib-based fixation, side-by-side axial connectors, and no crosslinks. The superior anchor foundations are outlined in the orange boxes where the anchors (screws or hooks) are fixed to either the spine or ribs. The inferior anchor foundations are outlined in the green boxes where the anchors are fixed to the spine. The axial connectors are outlined in the blue, dashed boxes. The rods are cylindrical and run parallel to each other (not outlined or highlighted in the figure). Single rod constructs would only consist of one rod along one side of the spine. The optional crosslinks are identified by purple arrows. The axial connectors, anchors, and crosslinks come with set screws used to lock these components to the rod. 6

Figure 3: Example of rod fractures. Two rod fractures (yellow circles) in a pediatric growing rod construct as captured on X-ray. 8

Figure 4: Examples of the surface topography of fractured components (cross sectional view) used to determine the failure mechanism. Note: pictorial representations only. Top left- bending under low nominal stress. Top right- bending under high nominal stress. Bottom left- reverse bending under low nominal stress. Bottom right- torsion under high or low nominal stress. 11

Figure 5: Rod Contouring Measurements. The rod sagittal angle (α) is the angle of intersection of the tangents to the outer edge of the rod (blue dashed lines) minus 180 degrees (example: 160 degree measurement is reported as 20 degree rod sagittal angle). Maximum deflection (x) is the distance of the line between the inner arc of the rod at α and the line connecting the ends of the rod (green solid lines). The background of each photograph was taken with a ruler and the scale was set in ImageJ prior to taking measurements. 22

Figure 6: Failure Analysis of Rod Fracture Surfaces. a) Example of a fracture surface under a digital optical microscope (40x). The fractographic features determine each zone: Zone 1- the crack initiation site is located where the beachmarks (concentric semicircles) end; Zones 2 and 3- the fatigue propagation areas show signs of beachmarks and fatigue striations; and Zone 4- the final rupture area has a ductile, shear appearance. The posterior and anterior sides of the rod were identified. a) SEM image (500x) of Zones 2/3- fatigue propagation area. The arrow points to a fatigue striation in the direction of propagation. c) SEM image (200x) of Zone 4- final rupture area. 23

Figure 7: Survival Curve of Rod Material. Both the failed and intact groups were comprised of constructs of varying rod materials, but no significant difference

was found in material versus implantation time (Cobalt Chromium- red line, Stainless Steel- green line, Titanium- blue line).	31
Figure 8: Determination of the orientation of retrieved rods. The anterior side (blue arrow) of the rod was determined by the presence of concentric oval shapes where the rod interfaced with the saddle of a polyaxial pedicle screw. 180 degrees from the anterior side was the posterior side of the rod. The posterior side (red arrow) of the rod was determined by the presence of small oblong shapes that come in pairs where the rod interfaced with set screws used to lock the rod to the screw housing.	34
Figure 9: Failure Mechanism and Sub-Categories. a1 & a2) pure bending fatigue, b1 & b2) pure bending fatigue with stress concentration, and c1 & c2) pure bending fatigue with stress concentration and local overload (dimpled region denoted as “LO”). Images on left are an angled view of fracture surfaces (FS) with the crack initiation site on the posterior side (PS) of the rod in a red box under a digital optical microscope (60x) and images on right are SEM images (100x) of fracture surfaces (FS) at the crack initiation site (zone 1).....	35
Figure 10: Representative Radiographs from Each Failure Location Category. Left to Right: Mid-Construct, Adjacent to Tandem Connector, and Adjacent to Distal Anchor Foundation. A-P Views on top row and Lateral Views on bottom row. Mid-Construct failures occurred in the middle of the construct with no interconnecting component in the vicinity of the rod fracture. Rod fractures adjacent to the tandem connector occurred just above and/or below the edge of the tandem connector. Rod fractures adjacent to the distal anchor foundation occurred just above the pedicle screws. All rod fractures are circled.	39
Figure 11: Radiographs Showing Fractures on the Rods Anchored to the Concave Side of the Major Spinal Curve. The circle shows the rod that fractured first in a construct with two fractured rods. The rod with a smaller final rupture area (zone 4) was determined to have failed first compared to the rod with a larger final rupture area that failed second.	40
Figure 12: Progression from the ASTM 1717 test setup intended to assess fusion constructs to a test setup that was modified to accommodate a pediatric growing rod construct. The test blocks used in the modified setup can accommodate four pedicle screws at each end that are fully inserted into the block. The setup was modified with either tandem (pictured) or side-by-side connectors. The modified setup has an active length of at least 200 mm. Crosslinks may also be added to the construct configuration (not pictured).....	52
Figure 13: Stress experienced by a spinal rod under bending. The posterior (red arrows) and anterior sides (blue arrows) of a spinal rod experience different directions of stress during flexion motion. Note that the spinal rods were subjected to compression bending in order to simulate spine flexion on the bench (black arrows). All rod fractures initiated on the posterior side of the rod experienced tensile stress; this is also the side of the rod where stress concentrations caused by interconnecting components (e.g., set screws) are located.	53
Figure 14: Side view of test setup showing a bending moment on the rod. The axial compressive load (F) is applied to the test blocks (beige rectangles) at an offset	

distance (x) away from the spinal rod (grey cylinder). Therefore, the rod is subjected to a bending moment ($F \cdot x$). The pedicle screws are screwed into the test blocks (dashed black boxes) with the screw housing (solid black rectangles) outside of the blocks connected to the spinal rod. Bolts are inserted through the white circles to attach the test blocks to the fixturing on the mechanical testing machine.	54
Figure 15: A secondary mechanical bench model. A) A 4-point bending test was used with custom fixtures to prevent rod rotation and translation. B) The specimen was subjected to a superior span of 60mm and an inferior span of 120mm. C) After rod distraction, prior indentations from the tandem connector set screws were exposed but the spans remained constant.....	59
Figure 16: Rod fracture induced through a 4-point bending test. The fracture initiated on the posterior side of the rod, adjacent to a stress concentration (yellow circle) caused by an indentation made from a set screw, during a dynamic 4-point bending test.	61
Figure 17: Results from dynamic 4-point bending testing. This small study was designed to examine the effects of exposed indentations on the rod and did not include a change in the length of the rod. The green line delineates runout at 1 million cycles. The control group showed significantly longer fatigue performance than the experimental group. Therefore, exposed stress concentrations on the posterior side of the rod experiencing tension significantly reduces the fatigue performance of the rod.....	62
Figure 18: Sample load-displacement curve derived from MATLAB software for static compression bending tests. Stiffness was calculated using the 2% offset method. Yield load (pink circle) was the point where the offset (dashed line) intersected the curve (solid line). Peak load (blue circle) was based on the maximum load achieved at 50 mm total displacement.	73
Figure 19: Fatigue performance for each construct configuration was captured through the number of cycles to failure during dynamic testing. All constructs were tested until rod fracture. Groups that do not share a letter are significantly different. Crosslinks significantly decreased the fatigue life of the constructs. Side-by-side and tandem connectors, regardless of length, have similar fatigue lives.	76
Figure 20: Examples of rod fracture after fatigue testing. The rods fractured adjacent to the pedicle screw (A) in four construct configurations. The remaining two construct configurations had crosslinks, and the location of rod fractures shifted adjacent to the crosslink (B). In all cases, fractures initiated on the posterior side of the rod adjacent to a stress concentration caused by either the pedicle screws or crosslinks.	77
Figure 21: Graph showing displacement over time during fatigue testing. Displacement correlated to the type of axial connector, and the construct configurations with 80 mm tandem connectors (orange plus sign and blue star) allowed for the least amount of displacement. The groups with crosslinks (black triangle and orange plus sign) had similar displacements compared to their corresponding groups without crosslinks (red square and blue star, respectively).	78

Figure 22: The test setup is based on ASTM F1717, modified to accommodate a pediatric growing rod construct. The active length of the construct was different for the groups described in Phases I-III. 90

Figure 23: Results from dynamic compression bending. The index length group (blue square) has a 200mm active length based on rod lengths from our prior retrieval study. The fifth lengthening group (orange circle) has a 255mm active length and was included to evaluate lengthening alone without exposing indentations. The indentations group (purple X) has a 255mm active length and was included to evaluate indentations alone without lengthening. The serial lengthening group (green triangle) has an active length that changed every 50,000 cycles where indentations were exposed after each lengthening..... 95

Figure 24: Photographs of an in vitro rod sample where the rod is lengthened to expose indentations made by set screws from the tandem connector. Rod fracture occurred in this location in 62.5% of samples in Phase III..... 96

List of Abbreviations

EOS- early onset scoliosis

ASTM- American Society of Testing and Materials

UHMWPE- ultra-high molecular weight polyethylene

SEM- scanning electron microscope

FEA- finite element analysis

Chapter 1: Introduction of Scoliosis and Pediatric Growing Rod Constructs

Scoliosis is a deformity where the spine experiences lateral and rotational curvature in the sagittal and coronal planes [1, 2]. Scoliosis is classified into four sub-categories based on the etiology of the deformity: idiopathic, neuromuscular, congenital, and syndromic [3]. Idiopathic curves are of unknown etiology; neuromuscular curves are attributed to neuromuscular abnormalities (e.g., cerebral palsy); congenital curves are due to structural abnormalities of the spine and/or thoracic cavity (e.g. fused ribs); and syndromic curves are associated with syndromes/genetic mutations (e.g., Marfan syndrome) [4]. Onset and progression of scoliosis mainly occurs in a pediatric population that is clinically distinguished by the age of the patient: infantile (<3 years old), juvenile (3-9 years old), or adolescent (10-20 years old) [3]. Early onset scoliosis (EOS) is a term used to capture spinal deformities that start during early development stages of the child, i.e. typically before age 5 and no later than age 10 [3]. This research focused on younger patients in the infantile and juvenile groups that experience such spinal deformities at critical ages when the spine and thorax (ribs, sternum, and muscles) are developing [3, 5]. Epidemiological studies either combine the prevalence of infantile and juvenile patients with the prevalence of adolescents and/or adults or stratify the prevalence rate based on the specific type of scoliosis and age group of the patient. For example, the American Academy of Orthopedic Surgeons reported 68,000 out of 100,000 people with an adult spinal deformity, 2,500 out of 100,000 people with adolescent idiopathic scoliosis, and 100 out of 100,000 people with infantile or juvenile

idiopathic scoliosis [6]. Therefore, the prevalence of all etiologies of scoliosis in EOS patients is unknown.

Thoracic Insufficiency Syndrome, coined by Campbell et al, is a clinical diagnosis used to describe deformities that restrict lung expansion and chest wall excursion [7]. Consequently, EOS patients may suffer from Thoracic Insufficiency Syndrome in addition to other comorbidities, and have higher mortality rates due to cardiopulmonary complications [8-10]. Therefore, treatment for these patients is critical and potentially life-saving. Treatment strategies consist of either conservative (non-surgical) treatments or surgical interventions such as fusion and non-fusion options. Regardless of the treatment strategy, the primary goal is to arrest curve progression and ideally reduce spinal curvature in order to mitigate musculoskeletal and cardiopulmonary complications [11]. Cobb angle is a clinical tool used to assess the degree of spinal curvature from an X-ray (Figure 1) [12]. Conservative treatments such as observation, bracing, or casting are often prescribed before surgical interventions, but such treatment has been questioned regarding effectiveness in the EOS patient population [3, 13, 14]. While there is no universally agreed upon treatment strategy for EOS patients, there are several factors considered when determining whether surgery is appropriate: Cobb angle (> 40 degrees), patient age (< 10 years old), propensity for curve progression (e.g., low Risser score), and failed response to non-surgical treatments [3, 15, 16].

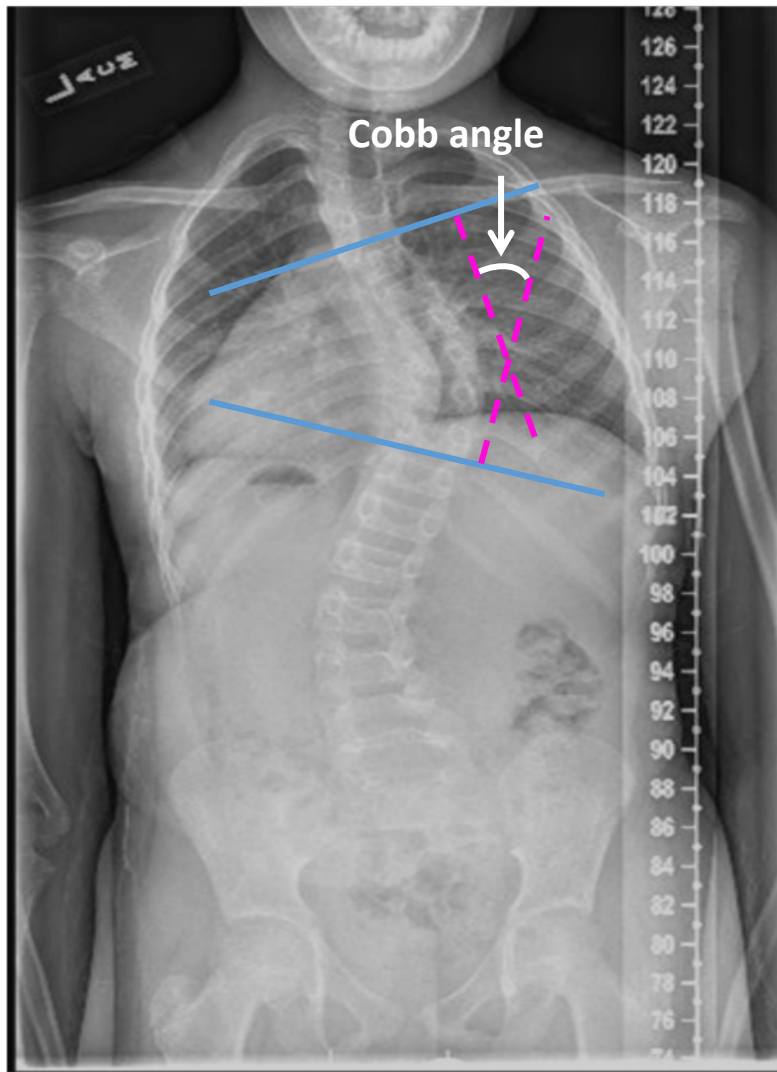


Figure 1: Measurement of Cobb angle on X-ray. Two lines (solid blue) are drawn parallel to the vertebrae at each end of a spinal curve. Two additional lines (dashed pink) are drawn perpendicular from the solid blue lines. The Cobb angle (white arc) is the angle at which the perpendicular lines (dashed pink) intersect.

Historically, fusion surgery was the gold standard to treat pediatric spinal deformities, but this surgical option has drawbacks in the infantile and juvenile populations. These drawbacks include the spine not reaching its maximum growth potential and/or experiencing crankshaft phenomenon where the fused spine has progressive rotational and angular deformity [17, 18]. In order to overcome the challenges with fusion surgery outcomes in children, the use of non-fusion surgical techniques were explored by reconfiguring the same implant components used in spinal fusion procedures but avoiding multi-level fixation to the spine with bone graft. The first documented non-fusion procedure was published in 1962 by a pioneering pediatric spine surgeon, Dr. Paul Harrington [19].

Since then, non-fusion surgical techniques in growing children (also known as growth-sparing or growth-guided techniques) have been refined and steadily gained popularity among pediatric spine surgeons [20-27]. In particular, spinal implants called pediatric growing rod constructs are commonly used devices given their advantages over spinal fusion and conservative treatments. Specifically, pediatric growing rod constructs allow for distraction across a non-fused portion of the deformed spine, followed by successive lengthening procedures every 6-12 months to encourage growth of the thorax and correction of the spinal curvature [28]. Thus, these devices are attractive surgical options for children at high risk for curve progression and cardiopulmonary insufficiency during the first 5 years of life when thoracic development occurs most rapidly [5].

There are several types of growing rod constructs: single rod with spine anchors, single rod with rib anchors, dual rod with spine anchors, and dual rod with rib anchors [3, 29]. All constructs have the same basic principles but differ in the selection of implant components and/or attachment points, which results in numerous possibilities for the construct to be configured. Each type of construct consists of the following implant components as shown in Figure 2: 1) superior anchor foundation above the primary curve that consists of screws and/or hooks anchored to the ribs or fused spine levels, 2) inferior anchor foundation below the primary curve that consists of screws and/or hooks anchored to fused spine levels, 3) rods that span across a non-fused portion of the spine, 4) axial connectors that facilitate rod lengthening (tandem or side-by-side connectors), and 5) optional crosslinks (also called cross connectors) that connect the longitudinal rods to increase torsional rigidity. The spine anchor points are the only parts of the spinal construct where the vertebrae (typically only two levels) are fused together to provide a strong foundation during construct distraction. The axial connectors, anchors (hooks and screws), and crosslinks come with set screws used to lock these components to the rod. The implant components are made from medical grades of either Titanium (commercially pure or Ti6Al4V alloy), Stainless Steel 316L, or Cobalt Chromium alloys (e.g., CoCrMo).

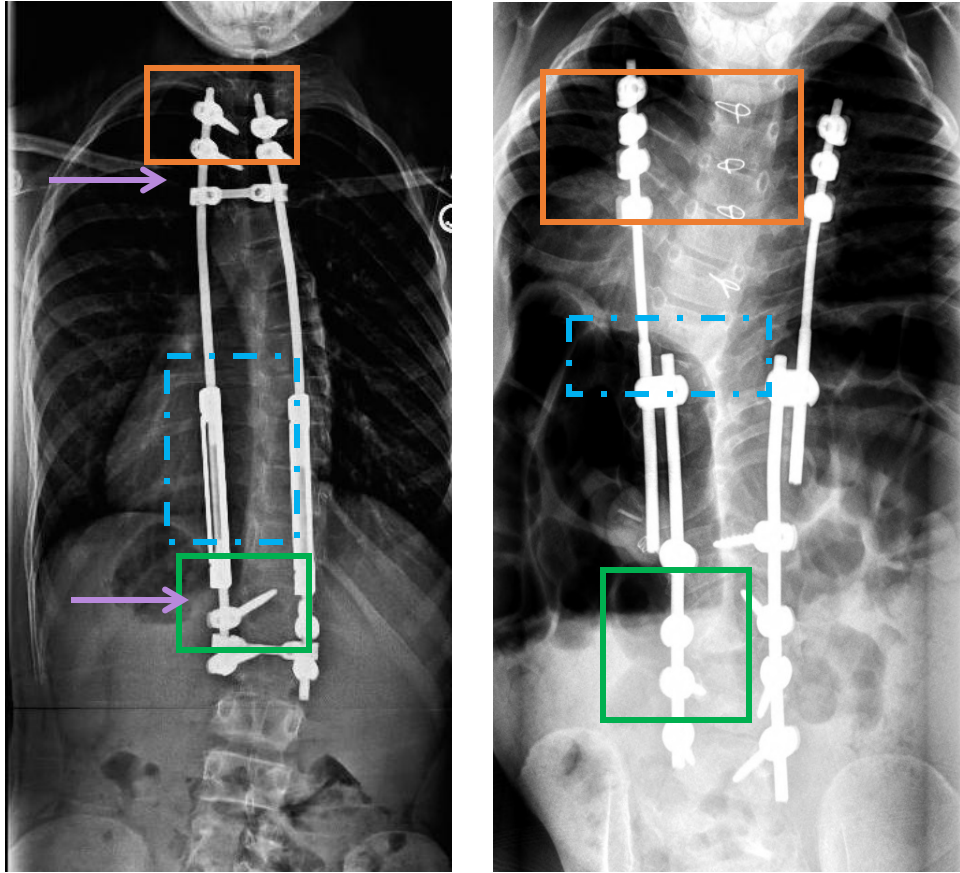


Figure 2: Types of implant components in growing rod constructs. Left: X-ray of a dual growing rod construct with spine-based fixation, tandem axial connector, and two optional crosslinks. Right: X-ray of a dual growing rod construct with rib-based fixation, side-by-side axial connectors, and no crosslinks. The superior anchor foundations are outlined in the orange boxes where the anchors (screws or hooks) are fixed to either the spine or ribs. The inferior anchor foundations are outlined in the green boxes where the anchors are fixed to the spine. The axial connectors are outlined in the blue, dashed boxes. The rods are cylindrical and run parallel to each other (not outlined or highlighted in the figure). Single rod constructs would only consist of one rod along one side of the spine. The optional crosslinks are identified by purple arrows. The axial connectors, anchors, and crosslinks come with set screws used to lock these components to the rod.

Despite their popularity, pediatric growing rod constructs suffer from complication rates as high as 72% [30], which often lead to unplanned reoperations for the patients in addition to planned lengthening operations. The types of complications include mechanical failure (e.g., rod fracture, dissociation), failure at the bone-implant interface (e.g., hook dislodgement, screw loosening), infection, implant prominence/skin irritation, and neurological injury.

Rod fracture (Figure 3) is one of the most common mechanical failures reported in the scientific literature with fracture rates ranging between 15% and 69%. This large range relates to the sample size used to collect rod fracture rates in each prior study. Prior studies involving smaller sample sizes (e.g., retrospective studies with less than 100 patients) typically reported higher percentages of rod fracture rates. Specifically, Bess et al reported 177 complications in 81 out of 140 patients (58%) where rod fracture occurred in 34/52 (65%) of patients [31]. Farooq et al followed 88 patients and found that implant complications included 31 rod fractures (35%) [23]. Sankar et al reported that 26 out of 36 patients (72%) had at least 1 major complication of which 18 were rod breakages (69%) [30]. Another study found 10 out of 16 patients (63%) experienced rod breakages of which 70% had multiple rod breakages [32]. Watanabe et al reported 119 complications in 50 out of 88 patients (57%) with 17 rod breakages [33]. Prior studies involving larger sample sizes (e.g., registry studies with several hundred patients) typically reported lower fracture rates. For example, Yang et al reported 86 rod fractures in 49 out of 327 patients (15%) with 16/49 patients (33%) having repeat fractures [34]. Rod fracture is an important focal point because it can be linked to pre-mature mechanical failure with direct

consequences to the patients being loss of device function and early device removal/replacement. However, the root cause of rod fracture is not well understood; therefore, this research focused on investigating the failure mechanism.

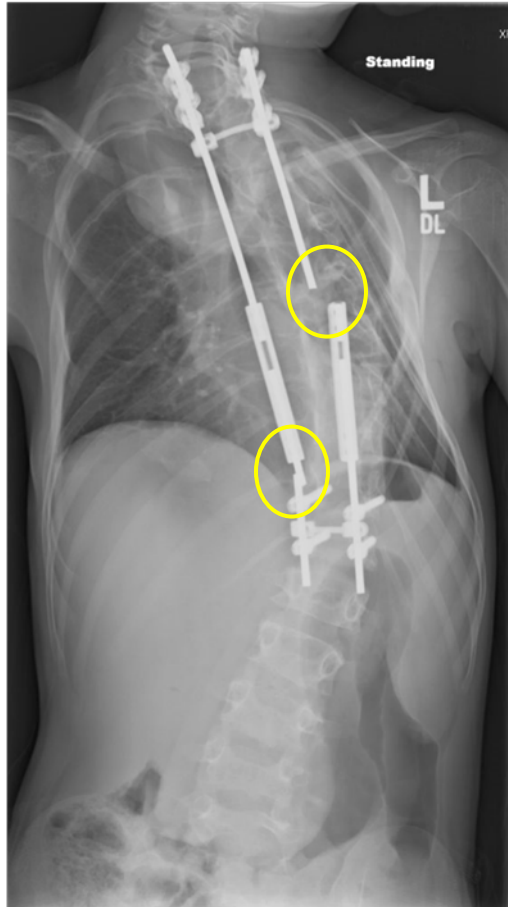


Figure 3: Example of rod fractures. Two rod fractures (yellow circles) in a pediatric growing rod construct as captured on X-ray.

A few prior studies provided insight into surgical, patient, and device-related factors contributing to complications in pediatric growing rod constructs, which provided the foundation for this research. Yang et al. presented a retrospective study comparing patients with a rod fracture vs. patients without a rod fracture [34]. The authors found there were several statistically significant differences in risk factors

between the two groups. Patients with rod fracture were more likely to have the following surgical or patient characteristics: syndromic scoliosis, pre-operative ambulation, and prior rod fractures. In addition, patients with rod fracture were more likely to have the following device characteristics: single rod constructs, stainless steel rods, shorter tandem connectors, and smaller diameter rods. Lastly, rod fractures occurred on average after the 4th lengthening. Watanabe et al. also performed a retrospective study to determine risk factors for postoperative complications for children with dual growing rod constructs [33]. The authors reported that three risk factors were found to be significant (and therefore associated with more complications) which included: ≥ 6 lengthenings, increase of every 20° in the proximal thoracic Cobb angle, and an increase of every 20° in the thoracic kyphosis angle. They also found that 50% of patients who had 5 or more rod lengthenings suffered from at least 1 complication. While this study did not evaluate as many device characteristics, it did show a similar result as the study from Yang et al where the number of complications increased with lengthenings. Yamaguchi et al. concluded that the pre-operative major coronal spine angle was the most influential risk factor for rod fracture [35], but additional factors were not correlated. In 2015, Yamanaka et al. performed a retrieval study of pediatric spinal instrumentation [36], which was the only prior investigation of the failure mechanism in this device area. However, their analysis was limited to one growing rod construct, thereby leaving room for a more robust investigation.

Most of these previous research studies on pediatric growing rod constructs reported only the device failure mode, which tells us *how* the device failed (e.g.,

fracture). However, it is important that we also understand *why* the device failed, also known as the failure mechanism (e.g., fatigue). Failure analysis is commonly employed across numerous fields, such as mechanical, aeronautical, and civil engineering in order to identify failure mechanisms of failed components. The goals of performing a failure analysis are to find the root cause of failure and prevent future failures of the same mechanism. Fractography is a technique within failure analysis where the topography of a fractured surface (cross section) is microscopically examined to determine how the fracture initiated and why it occurred [37]. The microstructure of the fracture surface provides details about the failure mechanism, and the overall surface topography of the failed component is compared to established failure mechanisms (Figure 4). Common failure mechanisms include fatigue, creep, wear, and corrosion. Fatigue failures, for example, can be further analyzed to provide answers regarding the direction of loading that caused the failure such as bending and/or torsion as shown through the examples in Figure 4. The direction of loading provides critical information about the *in vivo* loading conditions being experienced by the device, which will be useful for the development of a mechanical bench model.

The subject research investigated the failure mechanism of growing rod devices via a failure analysis to not only address limitations of the prior studies but, more importantly, to provide this information to the clinical community and device developers so that advances in device-based treatment options for scoliosis patients can be facilitated. More details regarding failure analysis will be discussed in Chapter 2. The failure mechanism for growing rod devices was investigated by: 1) collecting explanted devices and performing failure analyses to identify the failure mechanisms of

growing rod constructs, 2) analyzing radiographs (X-rays) and registry data to determine device, surgical, and patient characteristics that differ between patients with and without failures, 3) developing a mechanical bench model that can simulate failure, and 4) using the mechanical bench model to investigate the effect the unique characteristics of growing rod constructs have on mechanical performance.

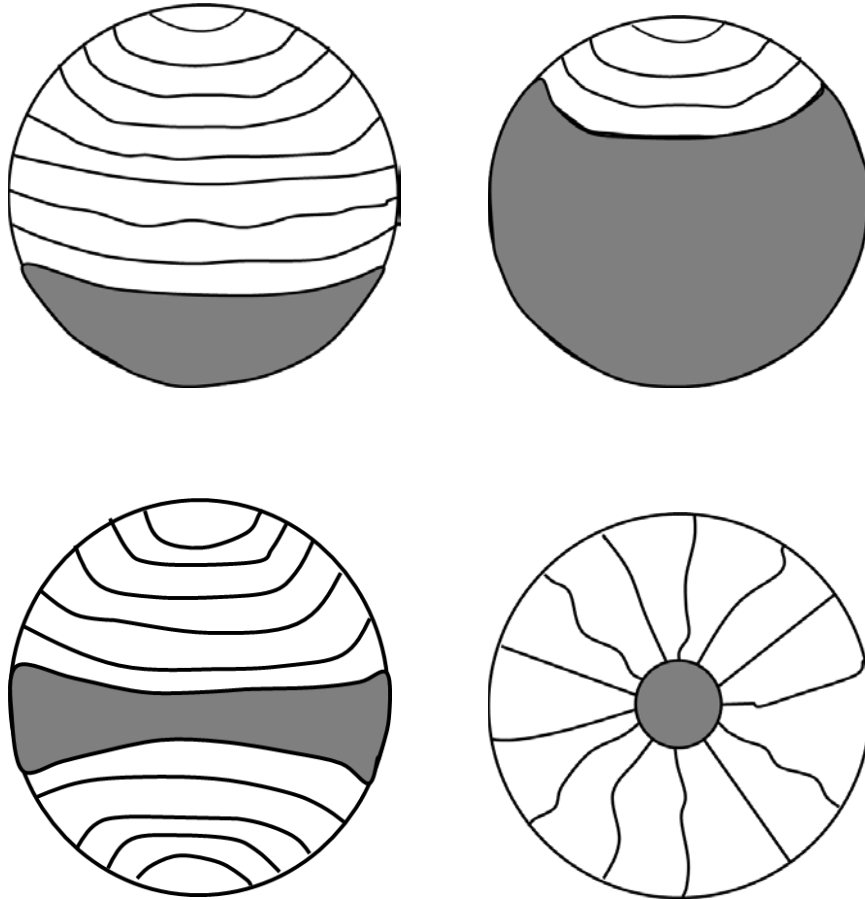


Figure 4: Examples of the surface topography of fractured components (cross sectional view) used to determine the failure mechanism. Note: pictorial representations only. Top left- bending under low nominal stress. Top right- bending under high nominal stress. Bottom left- reverse bending under low nominal stress. Bottom right- torsion under high or low nominal stress.

We collected and analyzed devices (known as explants or retrievals) that were removed from multiple patients at various clinical sites so that a comprehensive failure analysis could be performed. Based on the available literature regarding the configuration and failure of growing rods as well as knowledge of spine biomechanics, we hypothesized that rod fracture due to bending fatigue would be the most common failure mode/mechanism. We further hypothesized that crack initiation sites would be located near a stress concentration (e.g., indentation on the rod) created from prior lengthenings of the rod. Retrieved spinal implants are valuable resources since an assessment of the device surface can identify the mechanism(s) of failure directly. This information can then be used to properly mitigate the risk of rod fracture since we can answer both how and why the device failed.

The retrieval analysis was complemented by a radiographic analysis, which focused on determining differences in characteristics between patients with a failed device and patients without a failed device. X-rays allowed us to visually analyze the implanted construct, find the location and type of failure, and determine if there are any specific aspects of the construct or patient that may be associated with failure. Additionally, radiographic data was accompanied by registry data, which provided more patient and surgical characteristics such as demographics, diagnosis, weight, and ancillary measurements (e.g., hip symmetry). The retrieval, radiographic, and registry analyses enhanced our understanding of the *in vivo* loading conditions being experienced by the device and allowed us to establish parameters for a mechanical bench model.

Prior to this research, there were no established pre-clinical test methods or bench models to assess mechanical performance of pediatric growing rod constructs. *In vitro* testing is a valuable resource to the scientific and medical community as it permits for assessment of device performance under controlled laboratory conditions prior to human use by determining if a new device, device iteration, or surgical technique (i.e., implant configuration) may withstand simulated *in vivo* conditions. ASTM F1717 *Standard Test Methods for Spinal Implant Constructs in a Vertebrectomy Model* is one established test method for assessing the mechanical performance of spinal instrumentation [38]. However, this standard was developed to provide a repeatable test method for comparing spinal devices used in adult fusion populations where the spine has reached its growth potential and may not be deformed. Therefore, ASTM F1717 was not intended to assess performance of pediatric growing rod constructs with their own unique features or to recreate relevant clinical failure modes.

A mechanical bench model that is predicated on clinical outcomes can serve as a tool for engineers and researchers who are looking to improve pediatric growing rod constructs as it will enable them to make relevant predictions about the device's resistance to failure. This research aimed at developing a mechanical bench model for growing rod constructs that can simulate *in vivo* conditions and recreate a clinically relevant failure. More details on the development and validation of a mechanical bench model will be discussed in Chapters 3-5. We hypothesized that the mechanical bench model can distinguish between stronger and weaker constructs by showing quantitatively significant differences in mechanical performance (e.g., yield loads,

stiffness values, and fatigue limits) between the configurations linked to failure compared to the configurations not linked to failure. If researchers are able to improve growing rod constructs and/or understand the mechanical profile of different surgical techniques (e.g., construct configuration), this can help reduce the number of unplanned reoperations and thereby decrease the risks to the patient.

Chapter 2: Identification of the Failure Mechanism of Pediatric Growing Rod Constructs¹

Introduction

Traditional, distraction-based growing rod constructs are commonly used in surgical treatment of patients with early onset scoliosis [3, , 20, 39-42]. Children with severe and progressive deformities are offered surgical treatment to mitigate cardiopulmonary complications, maintain spinal growth, and arrest curve progression. Growing rod constructs allow for distraction across a non-fused portion of the deformed spine, and are lengthened periodically to encourage growth of the spine and thorax [43]. These constructs consist of anchor points constructed with pedicle screws and/or hooks, rods, axial rod connectors (tandem or side-by-side connectors), cross connectors (also known as crosslinks), and set screws. Constructs may differ in implant configuration or attachment levels, but have similar mechanical principles to maintain construct stability and allow for longitudinal distraction.

Growing rod treatment is associated with high complication rates, which often lead to unplanned reoperations [23, 30-34, 44, 45]. Although somewhat expected for a deformed, growing spine, one of the most common implant-related complication is rod fracture, which may lead to loss of device function. Previous studies have determined risk factors associated with complications for growing rod patients. Yang et al. found that patients with rod fracture were significantly more likely to have pre-operative ambulation, syndromic scoliosis, prior rod fractures, single rod constructs,

¹ As adapted from Hill, Genevieve, et al. "Retrieval and clinical analysis of distraction-based dual growing rod constructs for early onset scoliosis." *The Spine Journal* (2017).

stainless steel rods, shorter tandem connectors, and smaller diameter rods [34]. Watanabe et al. reported three significant risk factors contributing to more post-operative complications: ≥ 6 lengthenings, increase of every 20° in the proximal thoracic coronal spine angle, and an increase of every 20° in the thoracic kyphosis angle [33]. Yamaguchi et al. concluded that the pre-operative major coronal spine angle was the most influential risk factor for rod fracture [35]. However, these particular studies did not examine retrieved components in order to further explore complications, especially rod fracture. Previous studies that have examined retrieved implants focused on Harrington rods or the analyses were limited to corrosion or metal ion release [46-59]. Yamanaka et al. performed a retrieval study of spinal instrumentation, but their analysis was limited to one growing rod construct [36]. Therefore, conclusions about the failure mechanism are limited.

Therefore, the goals of this research study were to: 1) investigate the mechanism of failure for growing rod constructs using retrieved implants, and 2) perform an in-depth analysis on differences in patient, device, or surgical factors between patients with failed and intact growing rod retrievals. We hypothesize that rod fracture due to bending fatigue will be the most common failure mode/mechanism. Furthermore, crack initiation sites will be located near a stress concentration (e.g., indentation on the rod) created from prior lengthenings. By collecting and systematically analyzing retrieved devices and registry data from multiple patients, the results from this study may aid in decreasing the risk of fracture by providing the foundation for future development of mechanical bench tests. This

study may also help reveal why some patients experience device failure compared to others.

Materials and Methods

Source of Retrieved Devices:

Four clinical centers received approval from their respective Institutional Review Boards to collect retrieved implants over a one-year period. Patients with traditional, distraction-based growing rods who had his/her implant removed and were previously enrolled in a multi-center EOS registry were eligible after providing informed consent. Based on anecdotal information from collaborating surgeons, single rod constructs were no longer part of accepted practice. Therefore, the study included only dual-rod constructs. In addition, the participating clinical sites were instructed to send traditional, distraction-based growing rod constructs in order for the study to have a homogenous collection of retrievals. Other implants used in EOS patients such as the Vertical Expandable Prosthetic Titanium Rib (VEPTR®), Shilla™ Growth Guidance System, and MAGEC® Spinal Bracing and Distraction System were not collected. The registry (a repository of clinical data) is open to patients across 28 clinical centers with EOS and a major coronal spinal curve angle \geq 25 degrees. The four clinical centers for the current study were selected based on their patient volume and ability to carry out the necessary procedures associated with device retrievals. At the time of this study, there were a total of 1,455 patients enrolled in the registry; 887 of which had growing rod treatment.

Registry Analysis:

Registry data were obtained to determine patient and surgical characteristics such as diagnosis, weight, and radiographic measurements at the pre-operative, post-index, and pre-retrieval time points for those patients with a retrieved device. The registry was also used to gather dates of all planned and unplanned surgeries in order to calculate total treatment time (index to removal surgery) and time between both lengthening and removal surgeries. Radiographs, when available, were obtained at every time point throughout the patients' course of treatment to date. The X-rays were evaluated to determine implant configuration, failure and lengthening locations, and any radiographic measurements that were unavailable from the registry. Since patients with traditional, growing rod constructs undergo numerous surgical procedures (e.g., patient growth) and components are commonly exchanged, both the X-rays and registry data were used to track the implantation and removal of each retrieved rod in order to determine implantation time.

To determine if the retrieval cohort was representative of growing rod patients, the retrieval cohort was compared to patients in the registry database with dual, growing rod constructs with spine-based fixation that were treated during the same time period. Pre-operative characteristics and demographics (diagnosis, gender, age, weight, ambulatory status, major coronal spinal curve magnitude, maximum kyphosis, lordosis, and T1-S1 length) were compared. It is noted that the indications for the index surgery for patients in the retrieval study was a large curve (> 60 degrees) and/or a curve causing functional difficulty. The data were analyzed using two-sided exact tests (Fisher's Exact or Fisher-Freeman-Halton) for categorical data

and Chi-Square tests for continuous data to find statistically significant differences ($p \leq 0.05$). Complete case analyses were performed as missing data were not imputed. When the inclusion criteria used for the four clinical sites participating in the retrieval study were applied to the full registry, 351 patients were identified. The retrieval cohort was found to be representative of these 351 patients across all pre-operative characteristics and demographics with no significant differences found (Table 1, all p values > 0.1). It is noted that 66/351 (18.8%) patients had at least 1 rod fracture and 44/66 (62.1%) patients had repeat rod fracture.

	Retrieval Cohort n = 30 patients Mean ± Standard Deviation or %	Registry n = 351 patients Mean ± Standard Deviation or %	P value
Diagnosis	6 idiopathic (20%) 9 neuromuscular (30%) 13 syndromic (43%) 2 congenital (7%)	61 idiopathic (17%) 110 neuromuscular (31.5%) 124 syndromic (35.5%) 56 congenital (16%)	0.56
Gender	16 Female (53%)	219 Female (62%)	0.33
Pre-op Age	7.3 ± 3.0 years	7.2 ± 2.8 years	0.86
Pre-op Weight	22.7 ± 7.9 kg	21.2 ± 8.9 kg	0.33
Pre-op Major Coronal Spinal Curve Magnitude	73 ± 16°	76 ± 19°	0.35
Pre-op Max Kyphosis	44 ± 33°	53 ± 24°	0.15
Pre-op Lordosis	-49 ± 34°	-48 ± 21°	0.85
Pre-op T1-S1 Length	275 ± 48 mm	265 ± 50 mm	0.21
Pre-op Ambulation	24 (80%)	212 (60%)	0.23

Table 1: Patient Characteristics and Demographics of Growing Rod Patients in the Retrieval Cohort vs. Registry

Retrieved Device Analysis:

The retrievals were categorized as either failed or intact after a thorough analysis of the implant components, radiographs, and registry data. Constructs were included in the analysis if at least one rod was retrieved and registry/radiographic data were available at pertinent time points (e.g., index surgery). Constructs were assigned to the failed group if the implants showed any signs of mechanical failure (e.g., rod fracture), and constructs were assigned to the intact group if the implants did not exhibit signs of failure. The data were compared across groups using the same statistical methods cited above to determine if there were any differences in patient, surgical, or device factors. The analyses were performed on a per construct basis unless otherwise noted. Time to device failure was analyzed for each rod material where constructs in the intact group were considered censored at the time of implant removal.

All retrievals were analyzed per ASTM F561 *Standard Practice for Retrieval and Analysis of Medical Devices, and Associated Tissues and Fluid* [60] (Appendix 1). Non-destructive analyses included photographic documentation, dimensional analyses, and image analyses. Energy dispersive X-ray spectroscopy (JEOL USA JSM-6390LV, Peabody, MA) was utilized to reveal the material composition of implant components. Retrieved components were subjected to low magnification imaging using a digital optical microscope (Hirox-USA KH-7700, Hackensack, NJ) to identify areas of mechanical fracture, damage, and/or corrosion. Rod contouring (rod sagittal angle and maximum deflection) was measured using ImageJ software (National Institutes of Health, Bethesda, MD) (Figure 5) [61], and statistical analyses

were performed on a per-rod basis. Components that exhibited mechanical fracture were subjected to high magnification imaging using a scanning electron microscope (SEM, JEOL USA JSM-6390LV). A failure analysis was conducted by examining the topography of the fracture surface to identify the crack initiation site (zone 1), crack propagation area (zones 2 and 3), and final rupture area (zone 4) as shown in Figure 6. The failure analysis involved identifying fractographic features (e.g., fatigue striations), which were then correlated with published failure mechanisms [37]. Both fracture surfaces of the rod were analyzed, when possible, to confirm the failure mechanism, especially when features were not visible due to burnishing. For rods that exhibited fatigue fracture, ImageJ was used to calculate the percent of the fracture surface that was consistent with fatigue propagation (zones 1-3).

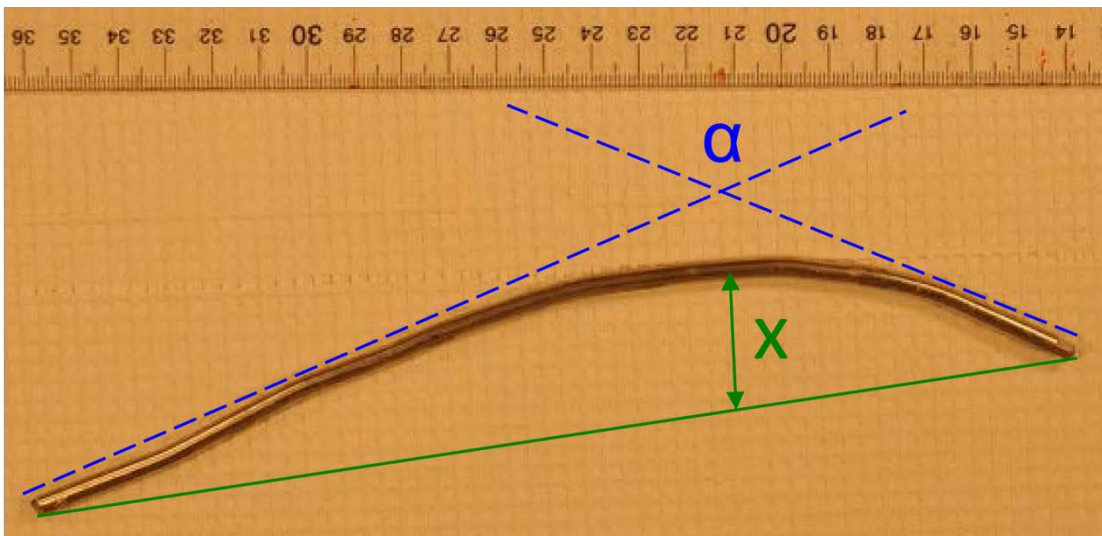


Figure 5: Rod Contouring Measurements. The rod sagittal angle (α) is the angle of intersection of the tangents to the outer edge of the rod (blue dashed lines) minus 180 degrees (example: 160 degree measurement is reported as 20 degree rod sagittal angle). Maximum deflection (x) is the distance of the line between the inner arc of the rod at α and the line connecting the ends of the rod (green solid lines). The background of each photograph was taken with a ruler and the scale was set in ImageJ prior to taking measurements.

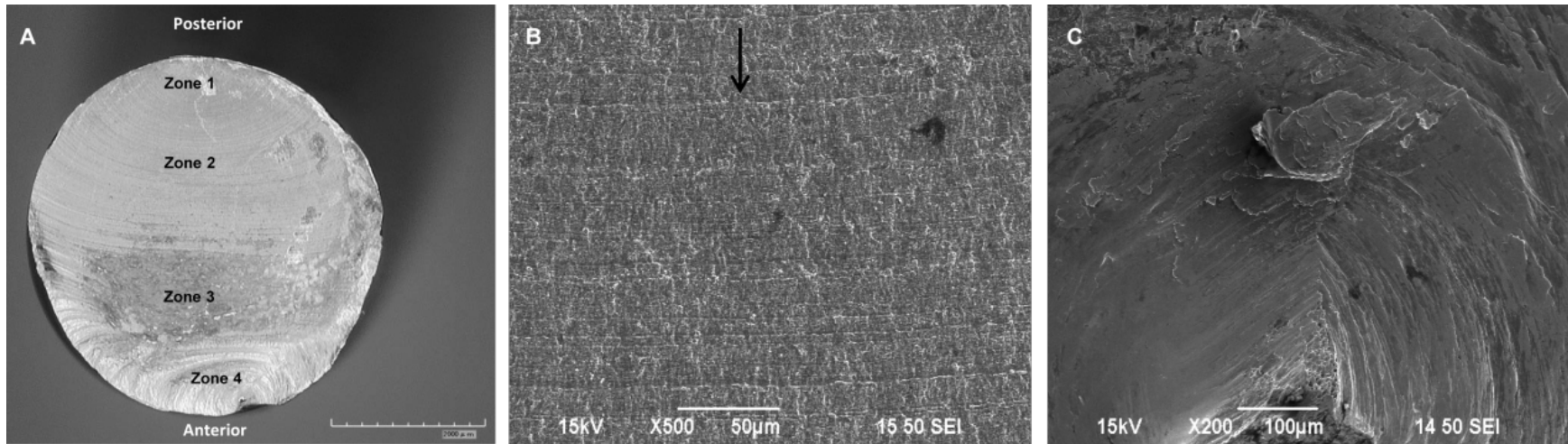


Figure 6: Failure Analysis of Rod Fracture Surfaces. a) Example of a fracture surface under a digital optical microscope (40x). The fractographic features determine each zone: Zone 1- the crack initiation site is located where the beachmarks (concentric semicircles) end; Zones 2 and 3- the fatigue propagation areas show signs of beachmarks and fatigue striations; and Zone 4- the final rupture area has a ductile, shear appearance. The posterior and anterior sides of the rod were identified. a) SEM image (500x) of Zones 2/3- fatigue propagation area. The arrow points to a fatigue striation in the direction of propagation. c) SEM image (200x) of Zone 4- final rupture area.

Results

Retrieval Collection:

Forty (40) dual-rod constructs were retrieved from 36 patients across four centers, with 18 constructs deemed as failures, 16 constructs deemed as intact, and 6 constructs did not meet the inclusion criteria. Three patients in the failed group had multiple sets of implants retrieved during the collection period; therefore, 18 failed constructs were received from 14 patients. All 18 constructs failed due to rod fracture, with 12/18 (67%) constructs having only one fractured rod and 6/18 (33%) constructs having two fractured rods in the same construct. Therefore, a total of 24 fractured rods were analyzed. The 16 intact constructs were removed due to final fusion/completed treatment (n = 7), implant exchange (n = 5), infection (n = 2), or implant prominence (n = 2). The types and quantities of retrieved implant components varied because only select components were removed during surgery (e.g., rod removed but screws remain implanted). As a result, the retrieved, failed constructs mostly consisted of rods alone without other construct components.

Comparison of Failed and Intact Retrieval Groups:

As shown in Table 2, the pre-operative characteristics and demographics were similar between patients in the failed and intact groups; the only exception being that the failed group was associated significantly with syndromic scoliosis (p = 0.009) when analyzed on a per patient basis. The remaining patients were diagnosed with idiopathic (3 intact, 3 failed), neuromuscular (8 intact, 1 failed), or congenital (2 intact, 0 failed) scoliosis. Beyond the pre-operative time point, a distinct difference

between the failed and intact groups was the number of prior surgeries for rod fracture. None of the patients in the intact group had surgeries for rod fracture in their course of treatment to date, including the seven patients that finished growing rod treatment. Conversely, in the failed group, 8/14 patients (57%) had at least one revision surgery due to rod fracture prior to the removal of the retrieved components, which was a significant difference between the groups ($p = 0.0005$).

Constructs in the failed group had more lengthenings than those in the intact group, though the comparison did not reach statistical significance: intact group: 3.8 ± 1.9 lengthenings; failed group: 4.8 ± 3.1 lengthenings ($p = 0.25$). The average time between lengthenings for the constructs in the intact group (9.4 ± 7.0 months) was similar to the failed group (10.0 ± 3.9 months) [95% CI (-4.5, 3.3); $p = 0.76$]. Total treatment time was also similar between the groups: intact group: 3.2 ± 1.8 years; failed group: 3.7 ± 1.9 years [95% CI (-1.7, 0.7); $p = 0.43$]. Implantation time of the retrieved components was 3.0 ± 1.9 years for the intact group and 1.7 ± 1.3 years for the failed group. However, implantation time for retrieved implants is expected to be shorter given patients with failed constructs had their rods exchanged more frequently due to prior revision surgeries for rod fractures. In the failed group, the average time between removal surgeries for rod fractures was 2.0 ± 1.3 years (range: 0.7 – 5.5 years).

	Failed n = 14 patients Mean ± Standard Deviation (Range)	Intact n = 16 patients Mean ± Standard Deviation (Range)	Mean Difference (95% Confidence Interval)	Two-sided P-value
Diagnosis	10 syndromic (71%)	3 syndromic (19%)	-52% (-76, -17%)	0.009
Gender	6 female (43%)	10 female (62.5%)	20% (-16, 51%)	0.46
Age	8.1 ± 2.6 years (2.7 – 10.7 years)	6.8 ± 3.3 years (1.7 – 13.1 years)	-1.3 (-3.3, 0.71)	0.21
Weight	22.4 ± 7.0 kg (11.1 – 38.5 kg)	23.2 ± 8.3 kg (9.2 – 40.9 kg)	0.8 (-4.4, 6.0)	0.76
Major Coronal Spinal Curve Magnitude	77 ± 14° (48 – 96°)	71 ± 17° (33 – 99°)	0.26 (-16.5, 4.5)	0.26
Max Kyphosis	37 ± 31° (-25 – 87°)	50 ± 33° (0 – 115°)	13 (-9.9, 35.9)	0.27
Lordosis	-58 ± 25° (-87 – 6°)	-44 ± 39° (-110 – 50°)	14 (-10.3, 38.3)	0.26
T1-S1 Length	281 ± 30 mm (206 – 323 mm)	272 ± 49 mm (180 – 347 mm)	-9 (-36.7, 18.7)	0.52
Ambulation	13/14 (93%)	11/16 (69%)	-24% (-51, 6%)	0.18

Table 2: Patient Characteristics and Demographics at Pre-Operative Time Point of Failed vs. Intact Retrieval Groups- Per Patient Analysis

Eight failed constructs were lengthened 2-4 times before experiencing their first and only rod fracture to date. The remaining ten failed constructs were lengthened between three and thirteen times over the course of treatment and overall experienced more rod fractures [3.6 ± 1.8 fractures (range: 2 – 7 fractures)]. When examining the number of lengthenings until the first rod fracture, two failed constructs experienced their first rod fracture prior to any lengthening surgeries, nine failed constructs experienced one lengthening prior to their first rod fracture, five failed constructs experienced 2-5 lengthening surgeries prior to the first rod fracture, and two failed constructs experienced eight lengthenings prior to their first rod fracture. For all additional rod fractures, no more than two lengthenings occurred between each rod fracture. The location of lengthening (e.g., cranial or caudal to the axial connectors) did not significantly associate with failure. Lengthenings occurred only cranial to the axial connectors in four intact constructs and one failed construct, only caudal to the axial connectors in three intact constructs and seven failed constructs, swapping between cranial or caudal to the axial connectors in seven intact constructs and seven failed constructs, and could not be determined in two intact constructs and three failed constructs.

No statistical differences between the groups were found when evaluating the change in patient characteristics between the pre-operative and retrieval time points. Therefore, post-index data were evaluated to determine if any differences were found between the groups when evaluating the post-index and retrieval time points. As presented in Table 3, the patients in the failed group had a greater change (increase)

in weight from the post-index to retrieval time points as compared to the intact group
($p = 0.02$).

	Failed n = 18 constructs Mean ± Standard Deviation (Range)	Intact n = 16 constructs Mean ± Standard Deviation (Range)	Mean Difference (95% Confidence Interval)	Two-sided P-value
Change in Age	3.5 ± 2.0 years (0.5 – 6.3 years)	2.6 ± 1.6 years (0 – 6.2 years)	-0.9 years (-2, 0)	0.15
Change in Weight	13.9 ± 10.7 kg (2.5 – 46.7 kg)	7.1 ± 5.4 kg (0 – 14.5 kg)	-6.8 kg (-13, -1)	0.02
Change in Major Coronal Spinal Curve Magnitude*	14 ± 15° (0 – 55)	13 ± 10° (0 – 30)	-1° (-10, 8)	0.82
Change in Max Kyphosis*	20 ± 14° (3 – 50)	14 ± 16° (1 – 59)	-6° (-17, 5)	0.28
Change in Lordosis*	17 ± 16° (1 – 50)	13 ± 12° (1 – 47)	-4° (-15, 7)	0.48
Change in T1-S1 Length*	42 ± 35 mm (2 – 137)	27 ± 25 mm (0 – 78)	-15 mm (-38, 8)	0.20

*Absolute values were taken for the change from post-index to retrieval time points

Table 3: Change in Patient Characteristics and Demographics from Post-Index to Retrieval Time Points of Failed vs. Intact Retrieval Groups

Both failed and intact groups were comprised of constructs of varying rod materials and diameters (Table 4), but there was no correlation with clinical outcomes in the retrieval cohort based on rod material or diameter. For example, the survival curve in Figure 7 shows no significant difference in material versus implantation time. In the failed group, the fracture surface of cobalt chromium rods exhibited the largest fatigue propagation area ($82.7 \pm 4.3\%$) followed by stainless steels rods ($77.2 \pm 12.5\%$). Titanium rods showed only $36.8 \pm 11.5\%$ of the fracture surface area as fatigue propagation, which was statistically different than cobalt chromium and stainless steel ($p < 0.0001$ for both).

Rod Diameter	# of Failed Constructs n = 18	# of Intact Constructs n = 16
Ø 3.5 mm	1	1
Ø 4.5 mm	9	11
Ø 5.0 mm	5	0
Ø 5.5 mm	2	2
Transition Rod: Ø 3.5 mm to Ø 4.5 mm	0	1
Mixture of Rod Diameters: Ø 4.5 mm and Ø 5.0 mm	1	1
Rod Material	# of Failed Constructs n = 18	# of Intact Constructs n = 16
Stainless Steel	7	3
Titanium	6	8
Cobalt Chromium	4	4
Combination of Stainless Steel and Titanium	1	1

Table 4: Rod Diameters and Materials in Failed and Intact Retrieval Groups

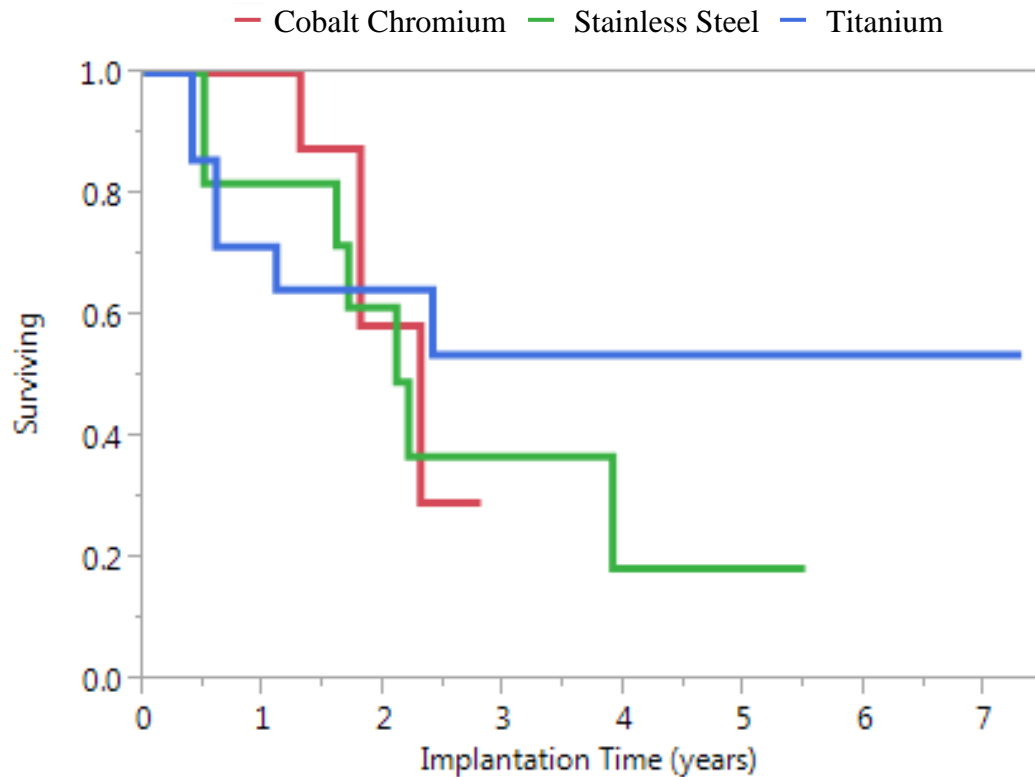


Figure 7: Survival Curve of Rod Material. Both the failed and intact groups were comprised of constructs of varying rod materials, but no significant difference was found in material versus implantation time (Cobalt Chromium- red line, Stainless Steel- green line, Titanium- blue line).

The retrieved rods showed signs of contouring. The rods in the intact group experienced more contouring, although not significant, with a rod sagittal angle of $25 \pm 16^\circ$ vs. $18 \pm 13^\circ$ in the failed group ($p = 0.08$), and maximum deflection of 10.2 ± 10.0 mm vs. 6.5 ± 6.3 mm ($p = 0.06$), respectively. No fractures were detected at the apex of the contoured rod in the failed group. Nine rods failed along the contour in the direction of spinal kyphosis, four rods in the direction of spinal lordosis, 10 rods failed in the transition area between kyphosis and lordosis of the spine (i.e.,

thoracolumbar junction), and one rod could not be determined due to missing radiographs.

Other device-related differences between the groups were the use of crosslinks and tandem connectors in the retrieved constructs. Only 3/16 (19%) constructs in the intact group included a crosslink and those cases showed only one crosslink present within the construct. Conversely, 17/18 (94%) constructs in the failed group included a crosslink ($p < 0.0001$), most of which included two to four crosslinks present within the construct. Nine intact constructs consisted of side-by-side connectors and seven consisted of tandem connectors. In comparison, two failed constructs consisted of side-by-side connectors and the remaining 16 failed constructs consisted of tandem connectors ($p = 0.009$).

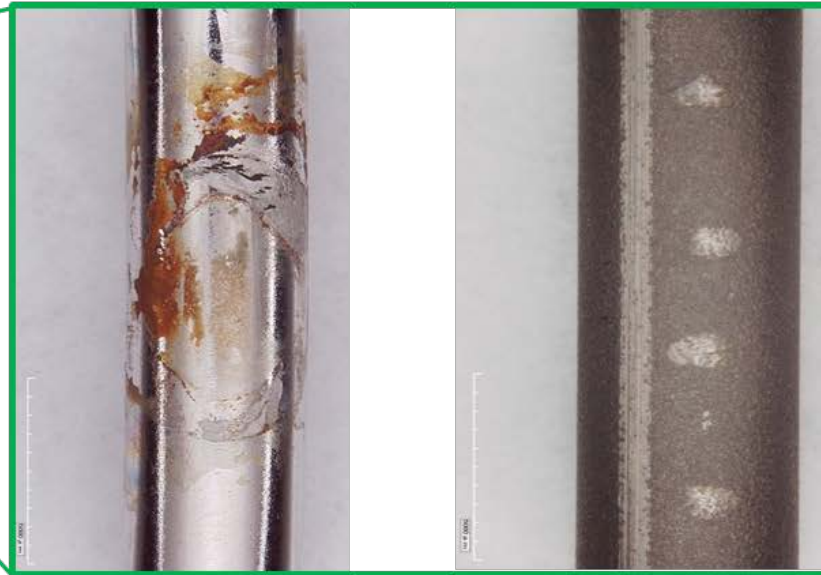
Failure Mechanism- Failed Group Only:

Imaging revealed that the failure mechanism for all 24 fractured rods was bending fatigue with crack initiation on the posterior side of the rod. Rod orientation was determined by reconstruction of the construct on the bench with supplemental information from the radiographs. For example, indentations from the saddle of the pedicle screw were observed on the anterior side of the rod and across from indentations caused by the set screw on the posterior side of the rod (Figure 8). Further analyses identified three sub-categories in the failed group: pure bending fatigue, pure bending fatigue with a stress concentration, and pure bending fatigue with a stress concentration and local overload (Figure 9). Fracture initiation was not linked to significant corrosion in any case, including the construct with dissimilar

materials (e.g., titanium screws and stainless steel rods). Therefore, corrosion (electrochemical oxidation of a metal that degrades the surface and can result in metal loss) was not concluded to be a major factor leading to failure. Additionally, wear (loss of material due to repetitive motion) was not determined to be a contributor to fracture initiation. Growing rod constructs may experience micro-motion between the interconnecting components, but further microscopic evaluation of the points of mechanical damage on the rod revealed that deformation and displacement of rod material caused an indentation on the rod rather than a loss of material.



Lateral view on X-ray of growing rod construct



Anterior side of rod that interfaced with the screw saddle

Posterior side of rod (180 degrees from anterior side) that interfaced with the set screws

Enlarged views of both sides of retrieved spinal rods

Figure 8: Determination of the orientation of retrieved rods. The anterior side (blue arrow) of the rod was determined by the presence of concentric oval shapes where the rod interfaced with the saddle of a polyaxial pedicle screw. 180 degrees from the anterior side was the posterior side of the rod. The posterior side (red arrow) of the rod was determined by the presence of small oblong shapes that come in pairs where the rod interfaced with set screws used to lock the rod to the screw housing.

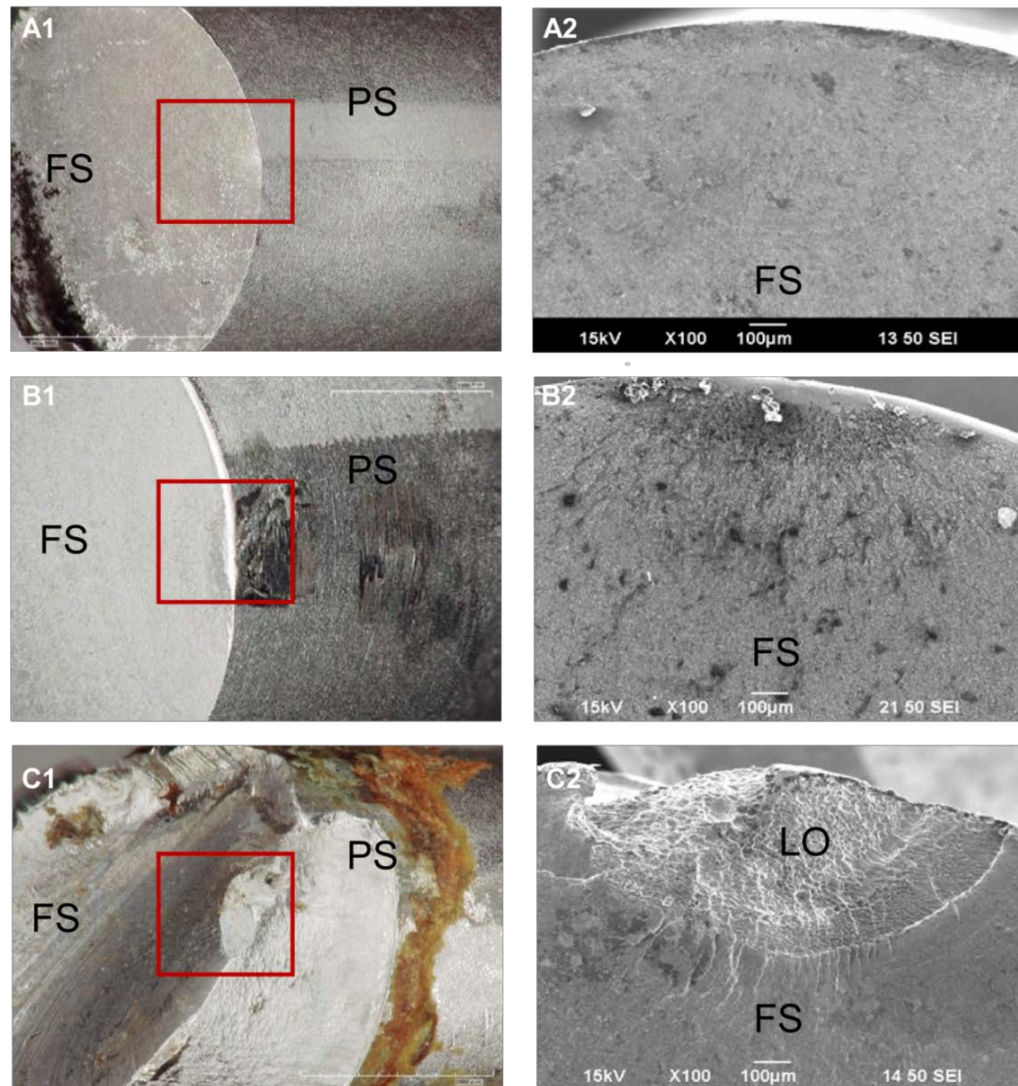


Figure 9: Failure Mechanism and Sub-Categories. a1 & a2) pure bending fatigue, b1 & b2) pure bending fatigue with stress concentration, and c1 & c2) pure bending fatigue with stress concentration and local overload (dimpled region denoted as “LO”). Images on left are an angled view of fracture surfaces (FS) with the crack initiation site on the posterior side (PS) of the rod in a red box under a digital optical microscope (60x) and images on right are SEM images (100x) of fracture surfaces (FS) at the crack initiation site (zone 1).

Rods from both the intact and failed constructs showed mechanical damage such as macroscopic stress concentrations at many points along the length of the rod surface, especially at locations where the rod was connected to another component within the construct such as a pedicle screw (Figure 8) or was in contact with an external object such as a tool. In 9/24 (37.5%) failed rods, these points of mechanical damage were not aligned with the crack initiation site and the rods failed in pure bending fatigue (Figure 9A1). These failures likely occurred due to the presence of an inclusion or material defect at the crack initiation site. In the remaining 15/24 (62.5%) failed rods, these points of mechanical damage were the source of stress concentrations. Fracture initiated at these stress concentrations as evidenced by the alignment of mechanical damage on the exterior surface (e.g., indentation) with the crack initiation site as shown in Figure 9B1 and Figure 9C1. Damage initiation at these locations subsequently led to fatigue fractures of the rod. In 5/15 cases where a stress concentration was detected in the failed rods, high magnification imaging revealed that the fracture surface had characteristics (e.g., dimpling) consistent with local overload failure just below the surface damage (Figure 9C2). Local overload failure occurs when stresses exceed the load-bearing capacity of the material [37].

The fractographic features on the fracture surfaces were consistent with published fatigue fracture patterns for high and low nominal stress scenarios [37]. The crack initiation site was identified by beachmarks that formed concentric semicircles around the initiation point (Figure 6A, zone 1). Crack propagation during fatigue was observed through beachmarks under low magnification imaging (Figure 6A, zones 2 and 3) and fatigue striations under high magnification imaging (Figure

6B), which verified that the rods failed due to fatigue. Final rupture was confirmed based on the transition from fatigue striations to ductile, shear areas (Figure 6A, zone 4 and Figure 6C).

Rods that failed in pure bending fatigue had the shortest implantation time of 1.1 ± 0.9 years compared to rods that failed in pure bending fatigue with a stress concentration and local overload (1.4 ± 0.9 years) or pure bending fatigue with a stress concentration (1.7 ± 0.4 years). There was no significant difference in implantation time for these three sub-categories ($p = 0.26$).

Fracture Location- Failed Group Only:

As outlined in Table 5 and Figure 10, radiographic similarities were found amongst failed constructs (e.g., device and patient features) based on the location of rod fracture: 1) mid-construct, 2) adjacent to tandem connector, and 3) adjacent to the distal anchor foundation. For example, mid-construct failures exhibited pure bending fatigue only and were retrieved from patients that had long constructs and more severe major curves. Failures adjacent to the tandem connector occurred in constructs that were implanted mainly in the thoracic spine and the connector length was similar to the individual rod length. Failures adjacent to the distal anchor foundation occurred above the cranial pedicle screw and the construct consisted of tandem connectors located at the thoracolumbar junction. In addition, rods that fractured adjacent to the distal anchor foundation showed the most consistent fatigue patterns as all fracture surfaces exhibited $> 60\%$ fatigue propagation area.

Similarities	Mid-Construct (4 constructs)	Adjacent to Tandem Connector (7 constructs)	Adjacent to Distal Anchor Foundation (5 constructs)
Axial connector location	Connector placed towards one end of the construct	Connector placed in the center of the construct	Connector placed at the thoracolumbar junction
Relationship between lengths of axial connectors and rods	Short connectors paired with long rods	Similar connector and individual rod length	Long cranial rods, long connectors, and short caudal rods
Construct length	Occiput or cervical spine to pelvis or sacrum	Upper thoracic spine to lower thoracic spine	Upper thoracic spine to lumbar spine
Coronal deformity	Pre-operative major curve magnitudes were ≥ 90 degrees	No similarities found	Pre-operative major curve magnitudes were 75-76 degrees
Failure Mechanism	Pure bending fatigue	Pure bending fatigue, pure bending fatigue with stress riser and local overload, and pure bending fatigue with stress riser	Pure bending fatigue, pure bending fatigue with stress riser and local overload, and pure bending fatigue with stress riser
Rod fracture was cranial or caudal to the apex of the major spinal curve	Caudal	Both Cranial and Caudal	Caudal
Rod fracture was cranial or caudal to the axial connector	Cranial or Caudal	Both Cranial and Caudal	Caudal

Table 5: Radiographic Similarities of Failed Constructs Based on Location of Rod Fracture

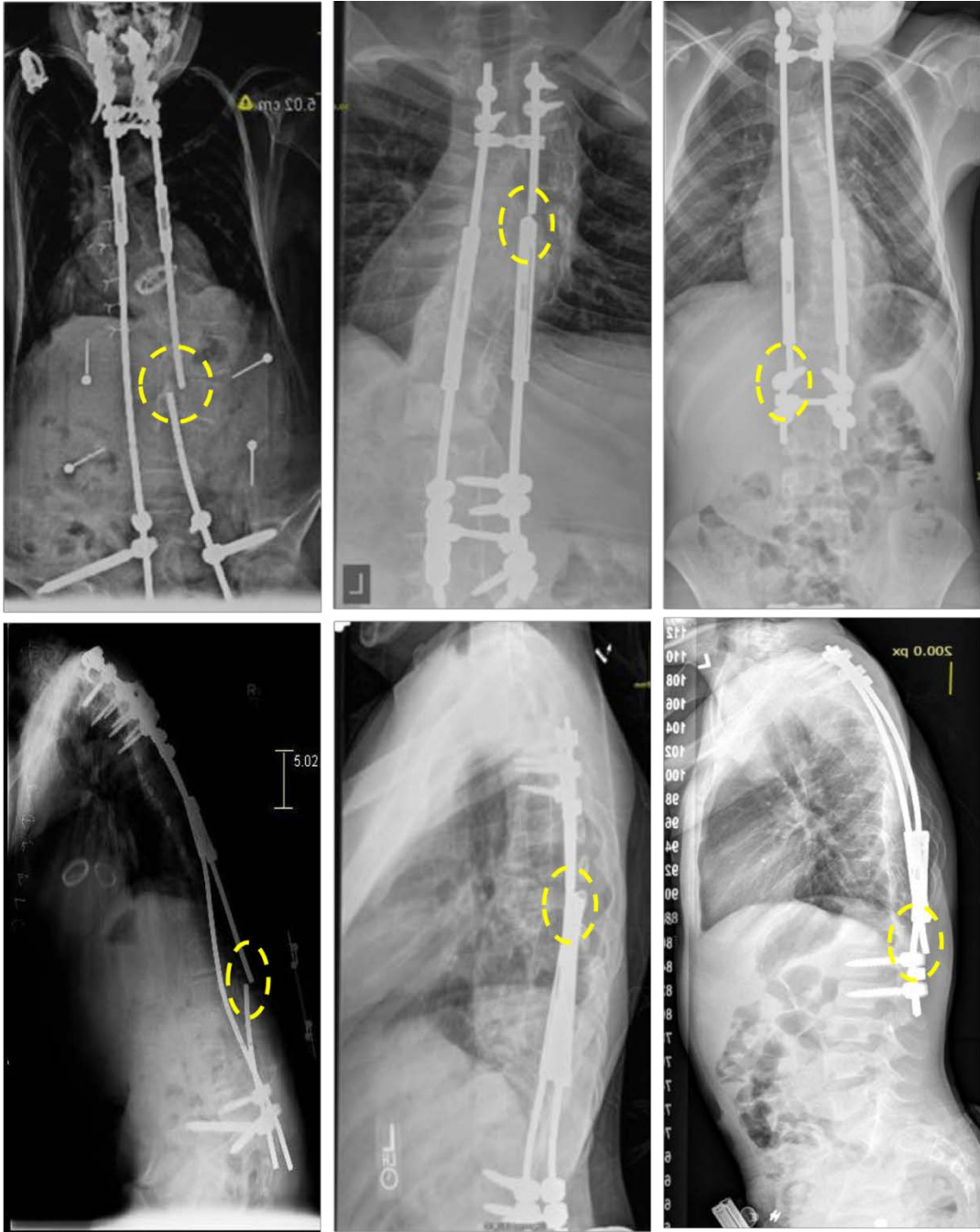


Figure 10: Representative Radiographs from Each Failure Location Category. Left to Right: Mid-Construct, Adjacent to Tandem Connector, and Adjacent to Distal Anchor Foundation. A-P Views on top row and Lateral Views on bottom row. Mid-Construct failures occurred in the middle of the construct with no interconnecting component in the vicinity of the rod fracture. Rod fractures adjacent to the tandem connector occurred just above and/or below the edge of the tandem connector. Rod fractures adjacent to the distal anchor foundation occurred just above the pedicle screws. All rod fractures are circled.

Of the 18 failed constructs, six constructs had fractured rod(s) above the axial connector, ten constructs had fractured rod(s) below the axial connector, one construct had one rod that fractured above the axial connector and a second rod that fractured below the axial connector, and one was unknown due to missing X-rays. Fracture occurred on the rod anchored to the concave side of the major spinal curve in 15/18 (83%) constructs (Figure 11). For patients that had two fractured rods within the same construct, the rod anchored to the concave side of the major curve failed first, which was elucidated by its smaller final rupture area.

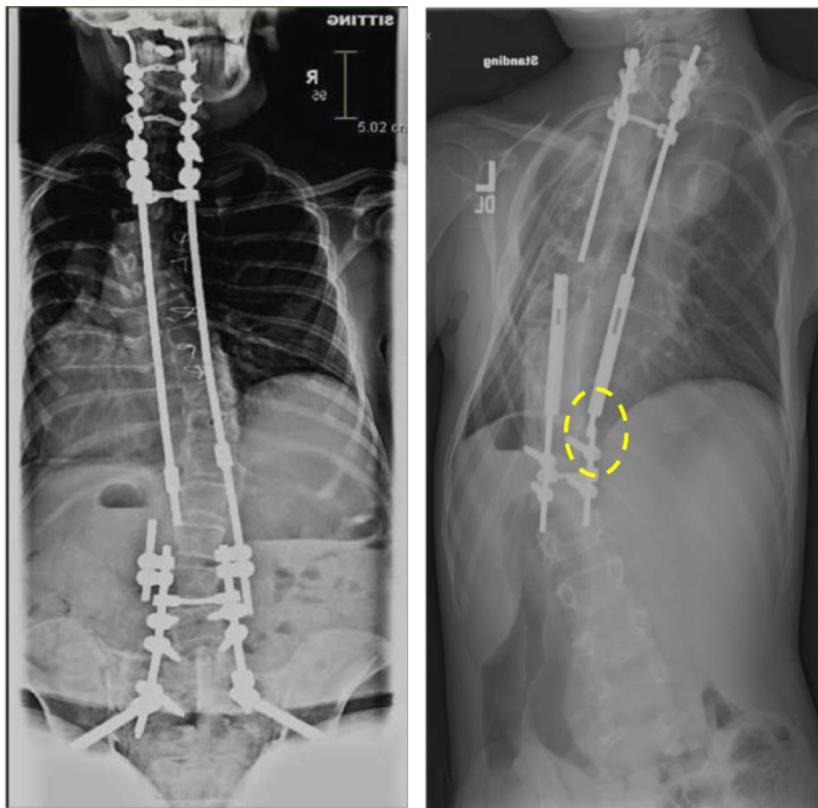


Figure 11: Radiographs Showing Fractures on the Rods Anchored to the Concave Side of the Major Spinal Curve. The circle shows the rod that fractured first in a construct with two fractured rods. The rod with a smaller final rupture area (zone 4) was determined to have failed first compared to the rod with a larger final rupture area that failed second.

Discussion

Traditional, distraction-based growing rod constructs are an important contribution to the treatment of spinal deformities of young children [3, , 20, 39-42]. These constructs are associated with high, device-related failure rates [23, 30-34, 44, 45], but the failure mechanisms have not been systematically researched. This is the first study to retrieve and analyze multiple growing rod constructs from several, high-volume centers, and to compare intact and failed retrievals. The results of this study show that bending fatigue in flexion is the mechanism of rod fracture, and that some rod fractures are initiated by high torques used during set screw insertion.

Additionally, this study revealed several factors associated with failure when comparing patients with failed and intact retrievals. These factors include syndromic scoliosis, prior rod fractures, rigid constructs with tandem connectors and multiple crosslinks, and increase in weight from the post-index to retrieval time points.

Syndromic scoliosis was significantly associated with the failed group in the current study and, was consistent with findings in previous studies [34, 62]. As outlined in Table 1, the registry data showed that growing rod constructs are used in EOS patients with all types of scoliosis. Specifically, 17% had idiopathic scoliosis, 31.5% had neuromuscular scoliosis, 35.5% had syndromic scoliosis, and 16% had congenital scoliosis. In addition, this study showed that patients with failed retrievals had significantly more surgeries for prior rod fractures, which is also consistent with a previous study [34]. Based on these results, frequent rod replacement should be considered in syndromic patients and patients with repeated rod fractures during

scheduled surgeries since these groups demonstrate a significant susceptibility to rod fracture.

Within the failed group, patients with more lengthenings had significantly more rod fractures. Furthermore, after the first rod fracture, no more than two lengthenings occurred between each additional rod fracture. Our study is in agreement with prior studies reporting that four or six lengthenings were associated with more complications [33, 34]. From a mechanical perspective, construct lengthenings increase the bending moment on the rod [63]. If the rod is not exchanged during lengthenings, larger bending moments can accelerate fatigue crack growth. Therefore, rod replacement for patients undergoing numerous lengthenings may aid in reducing the risk of rod fractures.

The combined use of tandem connectors and multiple crosslinks were found to be associated with failed constructs compared to intact retrievals. The failed constructs were typically configured with tandem connectors, 1-2 crosslinks at the distal end (above the pedicle screws), and 1-2 crosslinks at the proximal end (below the pedicle screws). In contrast, the intact constructs were typically configured without crosslinks (if a crosslink was present, there was only one at the distal or proximal end) and with side-by-side or tandem connectors. Prior studies have demonstrated how crosslinks increase torsional rigidity of spinal instrumentation [64-69]. While torsional rigidity may be useful for patients with instabilities, Serhan et al discuss the importance of strategic placement of crosslinks within the construct in regards to fatigue performance [70]. Yamaguchi et al. hypothesized that less rigid constructs allow for more mechanical slop and, therefore, were associated with a

lower incidence of rod breakage [35]. Using the same theory, the combined use of tandem connectors and multiple crosslinks in a spine-anchored system leads to a rigid construct that is resisting spinal loading as opposed to a less rigid construct that allows for deformation and mechanical slop and which adjusts to spinal loading. Our findings of the combined use of tandem connectors and multiple crosslinks in the failed group lend credence to this theory. It is noted that larger, prior studies did not find statistical difference between tandem and side-by-side connectors when examining registry data [34, 71]. Therefore, the differences identified here may be a limitation of the smaller sample size in our retrieval study. However, the prior studies did not assess the combined use of axial connectors and multiple crosslinks; thus, future studies should aim to understand the balance between construct rigidity and mechanical slop.

The current retrieval analysis revealed that the failure mechanism for all fractured rods was bending fatigue with crack initiation on the posterior side of the rod (failed group only); therefore, the analysis indicates that repeated flexion motion is the dominant mode causing rod failure over time. Despite the complex, three-dimensional stresses of a deformed, growing spine, the fracture surfaces did not display features consistent with torsional, lateral bending, or shear loading that would be associated with patient movement. The failure mechanism is consistent with the results from a previous retrieval study of one growing rod construct, which identified that the rod fractured in fatigue [36]. These findings will aid the future development of mechanical bench tests and computational models to predict rod fracture in

growing rod constructs, including magnetically-controlled implants that would be subjected to similar bending fatigue loads.

Furthermore, this study found that rod fractures occurred at one of three locations (mid-construct, adjacent to tandem connectors, and adjacent to the distal anchor foundation), and there were similarities in the patients/constructs in each category. All rods that fractured mid-construct had a long, unsupported length, which may have resulted in large bending moments during flexion motion leading to bending fatigue failure. For rods that fractured adjacent to tandem connectors, we hypothesize that the abrupt transition between the tandem connector and rod creates a stress concentration due to differences in stiffness between components likely from variations in geometry and material properties. This failure location was consistent with the results from previous studies of growing rod constructs, which identified that rods fractured in the vicinity of a tandem connector [36]. For rods that fractured adjacent to the distal anchor foundation, multiple components are clustered together at the distal end of the construct creating a stiff, rigid segment at fused spinal levels. We hypothesize that repeated flexion motion created a cantilever effect where the rigid end experiences the highest bending moments and shear forces. Thus, construct configuration and biomechanical loading led to high bending stress regions on the rod at each location resulting in fracture.

Stress concentrations play an important role in fatigue crack initiation. However, the presence of stress concentrations alone is not predictive of failure since intact rods also consist of stress concentrations. This study shows that high bending stress regions of the construct are dictated by its configuration (and patient factors),

and that the combination of stress concentrations within those high bending stress regions can contribute to rod fracture. For example, 80% of rods that fractured adjacent to the tandem connector and distal anchor foundation initiated at a stress concentration within a high bending stress region of the construct. Inspection of the rods' surface damage revealed that stress concentrations can be caused by pedicle screws, axial connectors, crosslinks, or iatrogenic damage. In severe cases, high torques used to insert set screws may locally overload the rod, which consequently produced an initiation point for crack progression and ultimately fatigue failure. Previous *in vitro* studies have discussed the concept of notch sensitivity in spinal rods, and found that damage created using rod contouring tools decreases fatigue life [72-76]. The current study, however, showed that stress concentrations originate from several sources and are not exclusive to rod contouring tools. These previous studies also showed that rod fracture occurs along the contour of the bend, whereas this retrieval study did not identify any fractures at the apex of the contour where the highest strain is expected after rod contouring. Future studies with the use of computational models provide an opportunity to explore patient and device factors that influence bending stress location or magnitude along the construct. For example, the model can reveal the stresses on the concave-anchored rod to help elucidate why these rods experience a higher percentage of fracture compared to the convex-anchored rod. Additionally, bench studies may help reveal the magnitude of insertion torques that cause overload failure on the rods.

A number of analyses were either unable to be performed or did not reveal statistical significance, which highlights the limitations of a retrieval study. For

example, since the retrieved components mostly consisted of rods, the effect of set screw design on rod fracture could not be evaluated. Rod material, rod diameter, change in sagittal alignment, and length of axial connectors or rods are some examples of factors that were not correlated with the failed group, which may be due to smaller sample sizes as compared to what can be achieved in a registry study. It is noted that some reported results may not have direct clinical utility but are helpful for the development of pre-clinical assessments (e.g., fractography).

Conclusions

In conclusion, this is the first study to examine multiple, retrieved growing rod implants. Despite the limitations of a retrieval study, our analysis found that rod fractures are due to bending fatigue, and stress concentrations play an important role in rod fractures as they are frequently found at the initiation point within high bending stress regions of the construct. In severe cases, high torques used to insert set screws locally overloaded the rod. Therefore, the data have supported our hypothesis that rod fracture due to bending fatigue would be the most common failure mode/ mechanism, and that crack initiation sites would be located near a stress concentration (e.g., indentation on the rod).

Given that surgeons are concerned with costs and potential insurance reimbursement associated with frequent exchange of implant components, this study revealed several recommendations regarding surgical technique (e.g., spinal rod replacement) to justify costs while minimizing the risk of future rod fracture. Several sets of patients should undergo frequent exchange of rods during scheduled surgeries

to help prevent unplanned surgeries due to rod fracture. This includes patients with syndromic scoliosis, patients that undergo numerous lengthenings, and patients that experience prior rod fracture. Each group presented significant differences compared to the intact group, and thereby, was associated with an increased susceptibility to rod fracture. Thus, frequent rod replacement in these patients may reduce their risk of future fractures because a new rod is free of mechanical damage, crack initiation sites, or prior fatigue stress. In addition, it is recommended that surgeons use torque-limiting wrenches and/or not exceeding the prescribed torques when inserting set screws to prevent a local overload failure on the rod. The set screws are used to lock the pedicle screw to the rod, and surgeons have the option to either manually tighten the set screws using a screwdriver without torque readings (known as a white knuckle technique) or using torque-limiting wrenches provided by the manufacturer. These recommendations could prevent the instantaneous overload failure that occurs during set screw insertion that leads to fatigue fracture of the rod. The data herein will contribute to the development of improved construct designs and future testing methodologies (bench and computational) for pediatric implants, with the ultimate goal to reduce failure rates and unplanned revisions in this patient population.

Chapter 3: Bench Model Development and Validation

Bench or *in vitro* testing of medical devices serves as a useful and necessary system for evaluating basic performance attributes of the device and can be used to address questions pertaining to device safety. For pediatric growing rod constructs, it is crucial to evaluate their mechanical performance because these devices are linked to high device-related failure rates [23, 30-34, 44, 45], and non-clinical assessments are necessary to determine whether device designs are improved before implantation into the patient. However, there are currently no bench models prescribed for pediatric growing rod constructs.

When evaluating potential resources, the primary mechanical bench model for spinal instrumentation is described in ASTM F1717, which is a standardized test method targeted for devices used in fusion procedures for adults [38]. The ASTM F1717 standard outlines several distinct tests to assess mechanical performance of adult devices: static compression bending, static tensile bending, static torsion, and dynamic compression bending. The standard discusses that these loading modes are intended to “simulate the clinical requirements for the intended spinal location.” ASTM F1717 provides a good foundation for mechanical performance assessments of pediatric growing rods because our prior retrieval study (Chapter 2) revealed that all rods in pediatric growing rod constructs fractured in bending fatigue during flexion motion [77]. The construct testing simulates bending fatigue because the applied load is offset from the spinal rod, thereby creating a bending moment on the rod (Figure 15). Therefore, dynamic compression bending was chosen as the primary loading condition to simulate bending fatigue in pediatric growing rod constructs.

The configuration of the standard test setup was also considered when developing the mechanical bench model for pediatric devices. The ASTM F1717 standard test setup is based on a vertebrectomy, which is a surgical procedure involving the removal of one vertebra and two adjacent intervertebral discs in cases such as tumor resection. This procedure results in a gap between the proximal and distal vertebrae available for screw fixation; therefore, it creates a worst case scenario for mechanical loading of the spinal device because there is no loading sharing with a solid fusion mass between the points of screw fixation. The ASTM F1717 test simulates these conditions wherein screws are mounted to two ultra-high molecular weight polyethylene (UHMWPE) test blocks which represent the vertebrae, there is a gap between the test blocks, and the test blocks are fixed to the mechanical test system (Figure 12). The ASTM F1717 test setup provides a good foundation for mechanical performance assessments of pediatric growing rods since the ends of the construct are anchored into the vertebrae with pedicle screws, and there is a long span between the screws where the rods are not loading sharing with a solid fusion mass. Therefore, the standard test setup was modified to accommodate a pediatric growing rod construct (Figure 12) to determine if this bench model could replicate rod fracture as seen in our prior retrieval study (Chapter 2).

For the pediatric growing rod bench model, the UHMWPE test blocks were modified to accommodate four pedicle screws in each block instead of two screws as listed in the standard. This modification was made because growing rod constructs consist of anchor foundations, typically with four points of fixation at each end. The standard instructs the user to leave the neck of the screw shaft exposed given screw

neck fracture is a failure associated with some adult, fusion devices [78-80].

However, the setup was modified so that the pedicle screws were fully inserted into the block. This modification allows for as much load as possible to be transferred to the rod to help induce rod fracture, which is a common failure in pediatric devices [23, 30-34, 44, 45]. The standard test method specifies a 76mm active length, defined as the distance between the superior and inferior pedicle screws, for instrumentation used in the thoracolumbar spine. The modified test setup for growing rods included a longer active length based on average rod lengths obtained from the retrieval study. Pediatric growing rod constructs tend to be long constructs spanning multiple vertebral levels of the spine. For example, the retrieval study showed constructs can span from the occiput or cervical spine down to the lower lumbar or sacral spine. Therefore, the active length for the modified setup is defined as the distance between the interior pedicle screws and was set to 200mm or more. The last modification to the standard test setup included the use of axial connectors (tandem or side-by-side). It is noted that one set of modified UHMWPE test blocks included offset screw holes when using a side-by-side axial connector in order to keep the rods parallel to the applied load (Appendix 2). Crosslinks (also known as cross connectors) are optional components used to connect the longitudinal rods, and can also be included in the test setup when needed (not pictured in Figure 12).

The final consideration for the mechanical bench model was in regards to the orientation of the *in vitro* specimen. More specifically, we learned from our prior retrieval study that the indentations caused by the set screws associated with the pedicle screws or axial connectors were located on the side of the rod (posterior) that

experiences tension (also see Figure 8) [77]. Mechanics of materials principles were explored to help explain this finding as depicted in Figure 13. In this example, the spinal rod is analogous to a beam in bending. The stress of a beam in bending varies linearly from zero at the center (neutral axis) to maximum at the outer fiber of the beam. In other words, the beam in bending causes tensile stress on one side and compressive stress on the other side, starting from the neutral axis. Therefore, during flexion of the growing rod construct, the posterior side of the rod experienced tension and the anterior side experienced compression [81]. Based on principles of fracture mechanics, crack growth typically occurs under tensile stresses that pull the tip of crack open; during multiple fatigue cycles, this leads to final fracture. The proposed bench model allowed for the correct rod orientation so that the interconnecting components (screw or connector) interfaced with the posterior side of the rod that is experiencing tension, just as the rod would *in vivo*.

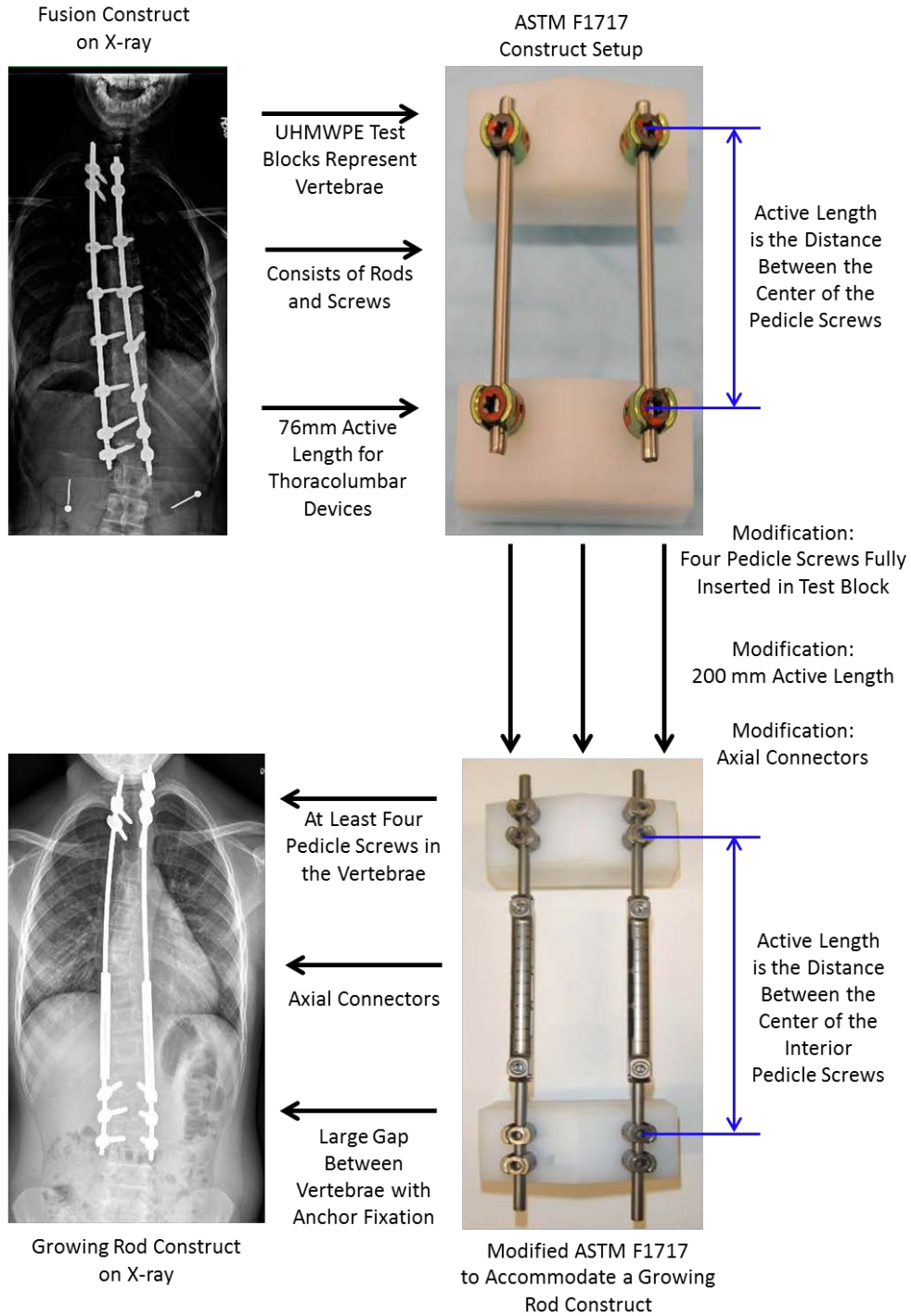


Figure 12: Progression from the ASTM 1717 test setup intended to assess fusion constructs to a test setup that was modified to accommodate a pediatric growing rod construct. The test blocks used in the modified setup can accommodate four pedicle screws at each end that are fully inserted into the block. The setup was modified with either tandem (pictured) or side-by-side connectors. The modified setup has an active length of at least 200 mm. Crosslinks may also be added to the construct configuration (not pictured).

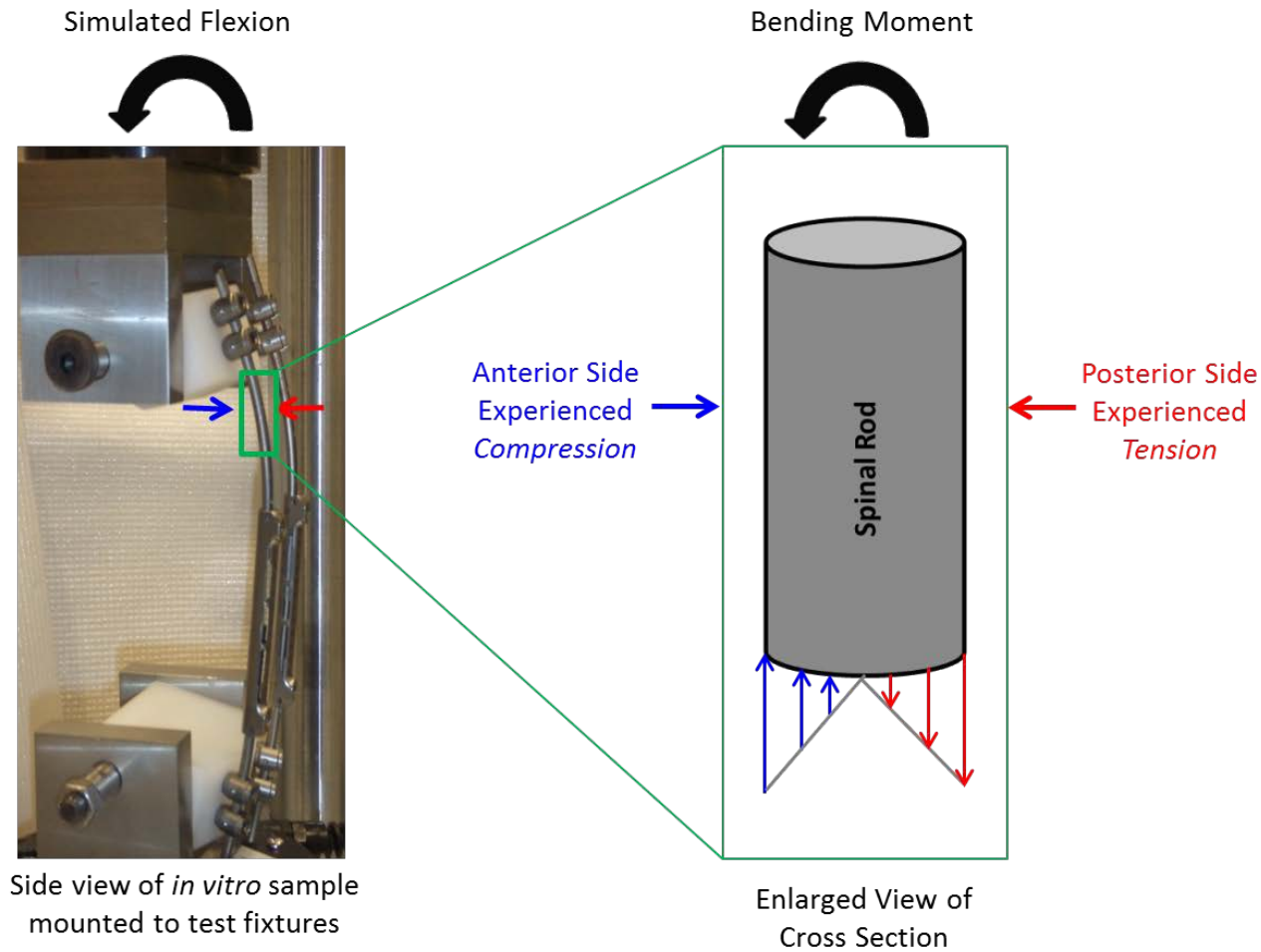


Figure 13: Stress experienced by a spinal rod under bending. The posterior (red arrows) and anterior sides (blue arrows) of a spinal rod experience different directions of stress during flexion motion. Note that the spinal rods were subjected to compression bending (via an offset axial load) in order to simulate spine flexion on the bench (black arrows). All rod fractures initiated on the posterior side of the rod experienced tensile stress; this is also the side of the rod where stress concentrations caused by interconnecting components (e.g., set screws) are located.

$$\text{Bending Moment} = F \cdot x$$

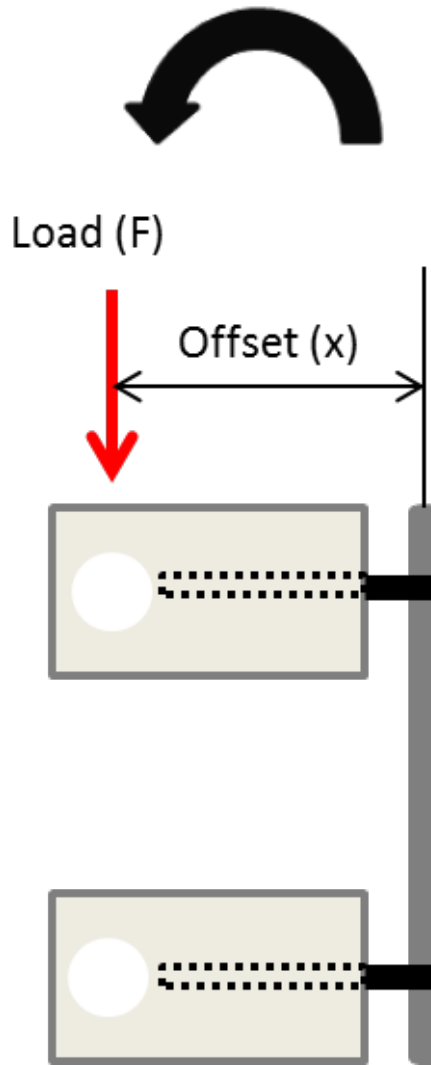


Figure 14: Side view of test setup showing a bending moment on the rod. The axial compressive load (F) is applied to the test blocks (beige rectangles) at an offset distance (x) away from the spinal rod (grey cylinder). Therefore, the rod is subjected to a bending moment ($F \cdot x$). The pedicle screws are screwed into the test blocks (dashed black boxes) with the screw housing (solid black rectangles) outside of the blocks connected to the spinal rod. Bolts are inserted through the white circles to attach the test blocks to the fixturing on the mechanical testing machine.

Validation experiments were performed to determine whether the failure mode (fracture) and failure mechanism (bending fatigue) in pediatric growing rod constructs could be replicated by the modified ASTM F1717 construct in compression bending. Prior to the validation experiments, static compression bending tests were performed to gather mechanical properties such as stiffness and yield load to help determine the parameters for the fatigue test. Static compression bending was done at a displacement-controlled rate of 25mm/min applied until a total displacement of 50 mm was achieved. The validation experiment consisted of a load-controlled dynamic compression bending tests performed at 4Hz between 150N and 15N ($R = 0.1$) per a sinusoidal waveform until rod fracture occurred. A calibrated mechanical load frame and load cell as well as custom fixturing were used to execute the testing. See Appendix 3 for standard operating procedures for mechanical testing. The failure mode and mechanism were identified on *in vitro* samples using the same failure analysis methods outlined in Chapter 2. The mechanical bench model was considered validated if it replicated the following conditions as exhibited through the retrievals:

- Rod fracture was induced.
- The fracture surface demonstrated signs of bending fatigue.
- The fracture initiated on the posterior side of the rod.
- Fracture initiation occurred in the vicinity of an indentation on the rod (e.g., stress concentration).

The results showed that rod fracture due to bending fatigue could be successfully replicated. These results were verified by examining the fatigue propagation areas through microscopy and comparing these areas to corresponding areas on the fracture surfaces of the retrieved rods (Table 6). The fatigue propagation areas from *in-vitro* and *ex-vivo* samples showed the same surface topography that was consistent with bending fatigue. In addition, the crack initiation sites showed that the *in-vitro* samples failed at indentations from set screws similar to the retrievals. Both the retrieved rods and bench samples demonstrated that rod fracture initiated on the posterior side of the rod as discussed in Figure 13. Therefore, it was concluded that dynamic compression bending test using the modified ASTM F1717 setup was an acceptable bench model to replicate failures seen clinically through retrievals.

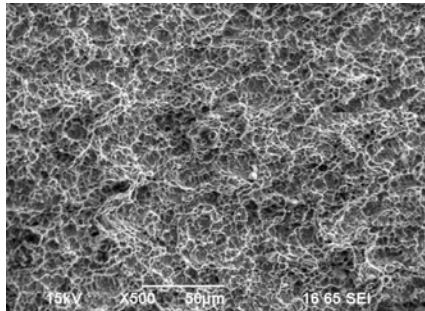
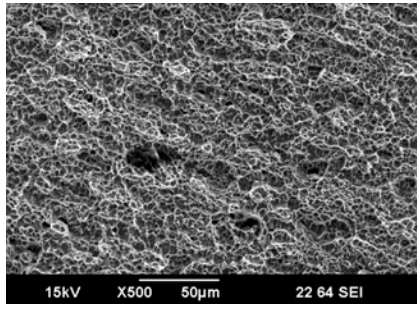
	Retrieval	<i>in-vitro</i> Sample
<p>Angled view of the crack initiation site</p> <p>(showing an indentation caused by a set screw)</p>		
<p>Fatigue propagation area</p>		

Table 6: Comparison of a titanium alloy retrieval to a titanium alloy *in vitro* sample to demonstrate validation of the mechanical bench model. Both spinal rods show crack initiation at a stress concentration and surface topography consistent with bending fatigue.

An additional bench model was explored to determine if rod fracture as seen in our prior retrieval study could be replicated. Although the modified ASTM F1717 model is acceptable, there may be cases where a simplified model is needed in order to isolate certain variables (e.g., stress on the rod versus the entire construct). A flexural bending test was considered to determine if it was feasible to achieve the same mechanism of rod failure but with fewer interconnecting components. Therefore, a 4-point bending test was created and adapted to accommodate a spinal rod with an axial connector (Figure 15). Four-point bending was chosen as the

flexural test because it can accommodate a spinal rod with an axial connector and undergo rod distraction while still applying a uniform bending moment as shown in Figure 15B-C.

Both static and dynamic bending tests were performed using this model on a calibrated mechanical load frame and load cell. Static bending tests were performed at a displacement-controlled rate of 2mm/min to gather mechanical properties. It was determined that 95% of the yield load was necessary to induce rod fracture during dynamic testing. Therefore, a load-controlled rate fatigue test at 5Hz between 570N to 57N compressive loads ($R = 0.1$) was performed per a sinusoidal waveform until rod fracture occurred. The setup involved the use of stainless steel rollers that spanned 120mm on the inferior end and 60mm on the superior end (Figure 15B-C). Custom fixture accessories such as four stainless steel dowels and two end plates were added to prevent rod rotation and translation (Figure 15A). A shorter tandem connector (e.g., 40 mm) or side-by-side connector could be used in this model. The axial connector faced downwards so that the posterior side of the rod experiences tension.

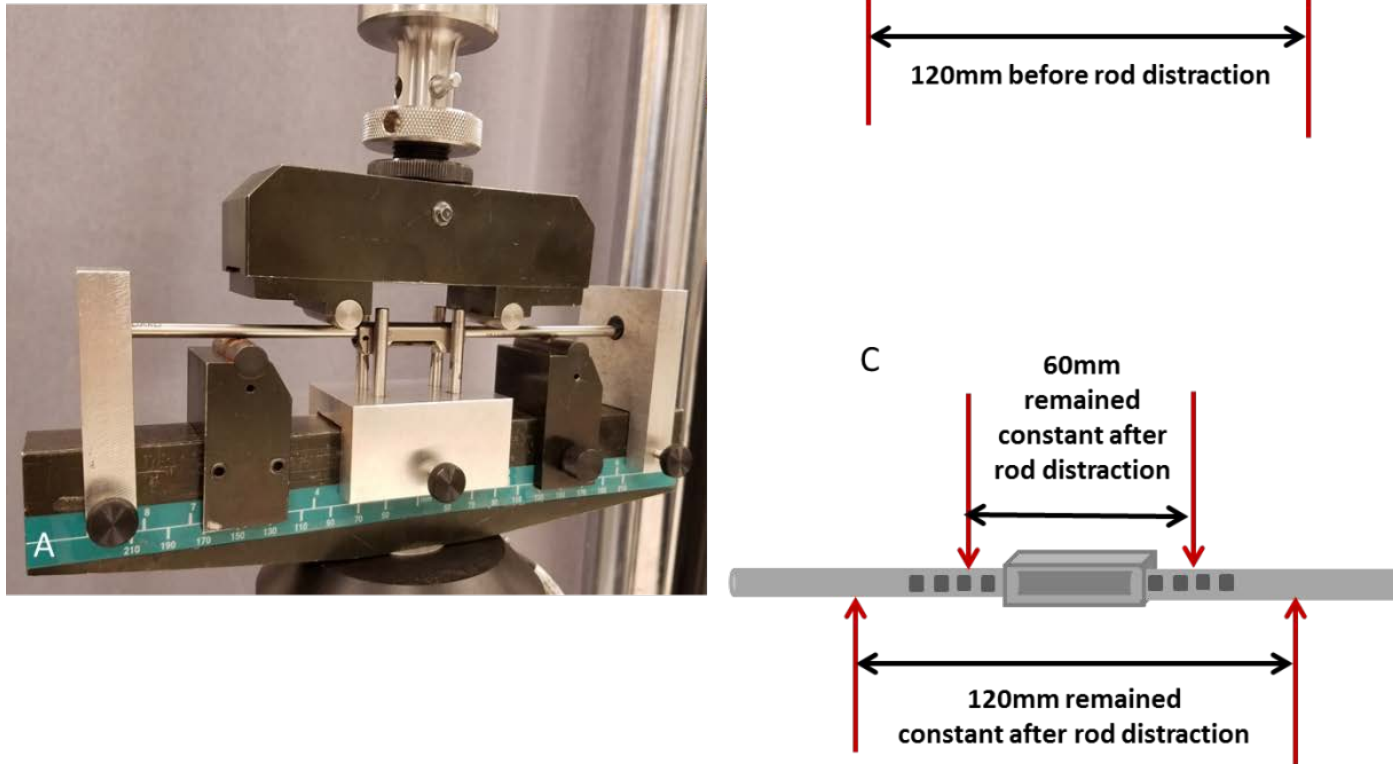


Figure 15: A secondary mechanical bench model. A) A 4-point bending test was used with custom fixtures to prevent rod rotation and translation. B) The specimen was subjected to a superior span of 60mm and an inferior span of 120mm. C) After rod distraction, prior indentations from the tandem connector set screws were exposed but the spans remained constant.

A small study was performed using this secondary mechanical bench model to investigate the impact of exposed indentations on mechanical performance of the rod in the absence of lengthening. Two test groups were compared, and both groups consisted of Ø4.5mm stainless steel rods and a 40mm titanium alloy tandem connector. The control group did not undergo rod distraction during testing and was fatigued until rod fracture or a runout of 1 million cycles; therefore, the control specimens did not have any exposed indentations. In contrast, the experimental group underwent a rod distraction every 50,000 cycles (4mm at each end of the tandem connector) to expose the prior indentations caused by the connectors' set screws. After the third and final rod distraction (maximum number achieved using a 40mm tandem connector), the specimens in the experimental group continued to be fatigued until rod fracture or a runout of 1 million cycles in total. It is important to note that the working length of the applied load was identical across the groups; therefore, increasing the length of the rod was not a variable (Figure 15B-C).

The results showed that rod fracture due to bending fatigue could also be successfully replicated through 4-point bending test using the same validation criteria as the construct bench model. In addition, the results demonstrated that fracture initiated on the posterior side of the rod, adjacent to a stress concentration caused by the set screw (Figure 16). Rods with multiple exposed indentations (experimental group) failed significantly earlier as compared to rods without exposed indentations (control group, Figure 17) in bending fatigue. The specimens in the control group reached runout of 1 million cycles ($n = 7$) or fractured just before runout between 900,000 and 1 million cycles ($n = 1$). The experimental group experienced rod

fracture in all cases before 410,000 cycles, and the rods fractured adjacent to a prior indentation created by the tandem connectors' set screws. In four of six specimens in the experimental group, rod fractures occurred at the exposed indentation created initially, i.e., furthest from the tandem connector. The remaining two specimens experienced rod fracture closer to the tandem connector at the indentation created during subsequent distractions. Therefore, it was also concluded that the flexural bending test was an acceptable bench model to replicate bending fatigue failures of the rod.

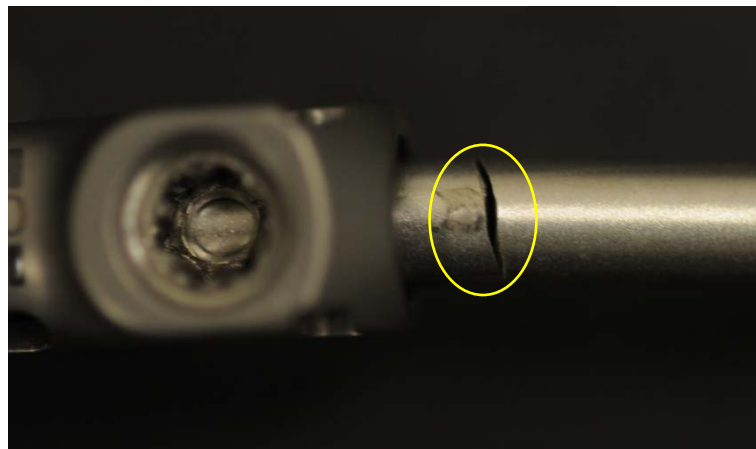


Figure 16: Rod fracture induced through a 4-point bending test. The fracture initiated on the posterior side of the rod, adjacent to a stress concentration (yellow circle) caused by an indentation made from a set screw, during a dynamic 4-point bending test.

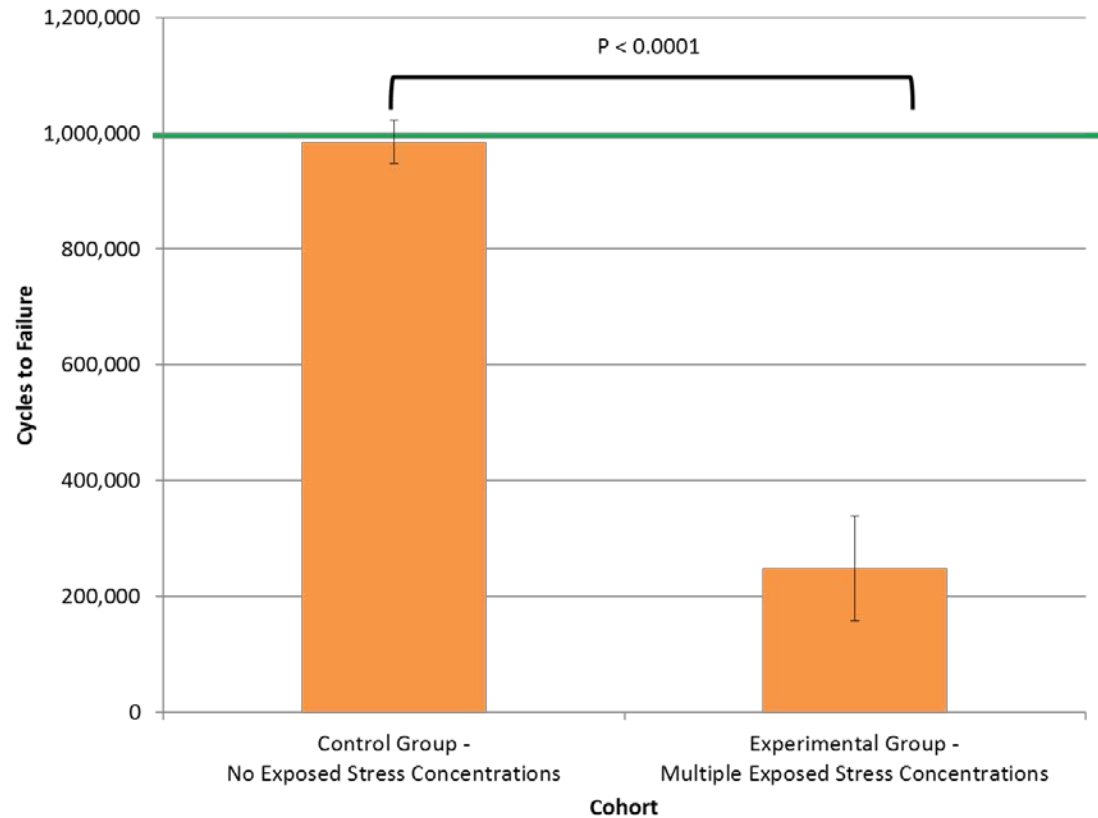


Figure 17: Results from dynamic 4-point bending testing. This small study was designed to examine the effects of exposed indentations on the rod and did not include a change in the length of the rod. The green line delineates runout at 1 million cycles. The control group showed significantly longer fatigue performance than the experimental group. Therefore, exposed stress concentrations on the posterior side of the rod experiencing tension significantly reduces the fatigue performance of the rod.

In conclusions, two mechanical bench models were successfully developed and validated for pediatric growing rod constructs. Both models are able to address unanswered questions related to the mechanical performance of growing rod constructs and their unique features. The models are similar in that they simulated bending fatigue and induced rod fracture on the posterior side of the rod in the vicinity of an indentation. One model, based on a modified ASTM F1717 setup, involved an entire pediatric growing rod construct where various interconnecting components can be interchanged. This model will be useful for examining construct complexity and how individual components or variables can impact the mechanical performance of the entire construct (Chapter 4 and Chapter 5). For example, this model can evaluate the difference of construct performance when using a tandem versus side-by-side connector. The second model, based on a 4-point bending test, is a simplified model that eliminates the variables from a construct test so that focused hypotheses on specific components can be tested. For example, this model can evaluate the performance of different rod materials that were subjected to mechanical damage from interconnecting components. While the second mechanical bench model is useful for future work, it was not explored further in this research given that construct testing was deemed to be most important for assessing overall device performance.

The mechanical models fulfill an unmet need as they can be used to address questions pertaining to device safety in an area where failure rates are high. However, the models present several limitations. First, the purpose of mechanical bench testing is to simulate *in vivo* loading experienced by the device; however, it is important to

note that the bench test method will not load the growing rod construct in exactly the same manner as it would be in the body. For example, the spine achieves motion in a complex manner through various directions of loading (flexion/extension, lateral bending, and torsion) across multiple vertebrae, intervertebral discs, and facet joints. However, the construct model simplified bending fatigue by applying an offset axial load in the proposed setup to simulate motion. Second, the models are not able to account for growth of the patient or correction of the spinal curvature. This is important because skeletal growth will place tensile stresses on the construct. We focused on compressive bending instead of tensile bending since the spine is primarily loaded in compression due to its function of supporting upper body weight. Future work is needed to understand the impact of skeletal growth on rod fractures in growing rod constructs. Third, the construct model was not able replicate the exact location of rod fracture from the retrieval study. Specifically, bench testing of three different construct configurations (Figure 10 and Table 5) could not replicate rod fracture that occurred mid-construct, adjacent to the tandem connector, or adjacent to the distal anchor foundation. Regardless of the configuration, rod fracture in the mechanical bench testing occurred adjacent to the pedicle screw instead so the model was not sensitive enough to replicate the fracture location; therefore, a computational model was deemed to be more suitable to address questions surrounding the prediction of rod fracture location. Lastly, the modified 1717 construct model is limited to growing rod constructs and was not developed or validated for other pediatric devices with a different principle of operation (e.g., spinal tethers).

Chapter 4: Investigation of Growing Rod Construct Complexity using the Mechanical Bench Model

Introduction

Traditional, distraction-based growing rod constructs used in children with early onset scoliosis (EOS) have unique features compared to spinal instrumentation used in adult or fusion applications. One unique feature of these constructs is the ability of the surgeon to utilize a variety of configurations to achieve rod lengthening via axial connectors and encourage growth of a deformed spine and thorax [3]. The axial connectors join the longitudinal rods either side-by-side in a parallel orientation (known as a side-by-side or wedding band connector) or in series where the rods are placed into each end of the connector (known as a tandem connector). Crosslinks, also known as cross connectors, are optional components used in the growing rod constructs to help increase the torsional rigidity by connecting the parallel longitudinal rods [64-69]. The surgeon's selection of the axial connector type or length as well as the quantity of crosslinks is primarily based on surgeon preference and patient anatomy, resulting in numerous possibilities of construct configurations. Given that growing rod treatment is associated with high complication rates [23, 30-34, 44, 45], it is important to understand the biomechanical differences between various construct configurations and the subsequent impact on device failure.

The relationship between rod fracture and construct configuration in traditional, distraction-based growing rod constructs is not well understood. As identified from a registry analysis, Yang et al. concluded that rod fracture was associated with "longer" tandem connectors, but the connector length was not reported [34]. Yamaguchi et al. hypothesized that less rigid constructs allow for more

“mechanical slop” (or flexibility) and, therefore, were associated with less rod breakage, but mechanical testing was not done to support this hypothesis [35]. The connector-rod interface was explored by Lee et al., but was limited to loosening only and did not include an evaluation of rod fracture [82]. Mahar et al. focused their investigation on biomechanical differences between anchor configurations and, therefore, did not evaluate the growing rod construct as a whole or correlate their findings with rod fracture [83]. In our previous retrieval study, it was reported that the combined use of tandem connectors and multiple crosslinks (2 or more) was associated with fracture of growing rod constructs while intact constructs were typically configured without crosslinks and with side-by-side or tandem connectors [77]. These prior studies indicated that certain configurations may provide better mechanical integrity over others, but more research is required to identify which construct components have the greatest impact on mechanical performance.

Therefore, a systematic investigation of construct complexity is necessary to determine the mechanical performance of various construct configurations. This need further necessitates the development of a novel non-clinical, mechanical model that can evaluate the complete construct and is representative of relevant spine biomechanical loading associated with fracture. Such a model is lacking from the literature. A non-clinical model is critical to help us understand the contribution of each implant component on the performance of the entire construct, which may help refine surgical techniques. In addition, the model can serve as tools for evaluating improvements in implant design.

The objective of the current study was to determine the mechanical performance of various configurations of traditional, distraction-based dual growing rod constructs with increasing complexity. To achieve this objective, the non-clinical model outlined in Chapter 3 was utilized to gather mechanical parameters of constructs with increasing complexity. We hypothesize that the mechanical bench model can distinguish between stronger and weaker constructs by showing quantitatively significant differences in mechanical performance (e.g., yield loads, stiffness values, and fatigue limits) between the configurations linked to failure as compared to the configurations not linked to failure.

Methods

Growing Rod Construct Configurations

In order to evaluate mechanical performance of growing rod constructs, a bench model that could subject the complete device, as opposed to individual components, to relevant spine biomechanics was needed. Therefore, the mechanical bench model was based upon compression-bending static and fatigue loading of spinal implants described in ASTM F1717 - *Standard Test Methods for Spinal Implant Constructs in a Vertebroctomy Model* [38], but the specimen setup was modified to accommodate growing rod devices. The specimen setup consisted of a growing rod components configured into ultra-high molecular weight polyethylene (UHMWPE) test blocks and loaded in compression-bending such that the posterior side of the rod was in tension. All device configurations included eight Ø4.5 mm poly-axial pedicle screws inserted fully into the test blocks (deviation from the

standard which outlines four screws that are not fully inserted), set screws, and bilateral Ø4.5 mm rods. Construct complexity was investigated by measuring the mechanical performance of six different configurations based on the types and lengths of connectors used (Table 7): 1) no connectors (rods only), 2) side-by-side connectors, 3) side-by-side connectors plus 4 crosslinks, 4) 40 mm long tandem connectors, 5) 80 mm long tandem connectors, and 6) 80 mm long tandem connectors plus 4 crosslinks.

The axial connectors were placed in the center of the construct, and the construct active length, which was measured as the distance between the interior pedicle screws, was consistent between all test groups at 200 mm (deviation from the standard that lists a 76 mm active length for thoracic, lumbar, and sacral constructs). The pedicle screws were located in the same location of the test blocks for all configurations, except the side-by-side connector constructs, which included offset screws in the superior test block in order to keep the rods parallel to the direction of applied load (deviation from the standard where all screws are centered in the test block). The construct configurations with crosslinks included two crosslinks at the proximal end and two crosslinks at the distal end for a total of four crosslinks in the high stress regions. The set screws were torqued to 60 in-lbs using a pre-set torque wrench. All components were made from Titanium alloy (Ti6Al4V) per ASTM F136 [84].

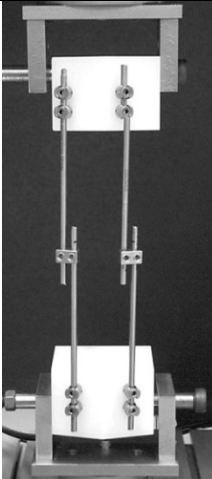
	No Connectors- Rods Only	Side-by-Side Connectors	40 mm Tandem Connectors	80 mm Tandem Connectors
Construct configurations <u>without</u> crosslinks				
Construct configurations <u>with</u> crosslinks	n/a		n/a	

Table 7: Photographs of the six construct configurations. The top row displays the constructs without crosslinks: No Connectors- Rods Only, Side-by-Side Connectors, 40 mm Tandem Connectors, and 80 mm Tandem Connectors. The bottom row displays the constructs with crosslinks: Side-by-Side Connectors Plus 4 Crosslinks, and 80 mm Tandem Connectors Plus 4 Crosslinks. All construct configurations have an active length of 200mm and the axial connectors are placed in the center of the construct (note: constructs with side-by-side connectors have offset pedicle screws in the superior test blocks). Fixtures include steel U-frames with pins attached to UHMWPE test blocks with the load cell on the bottom

Static Testing

Static compression bending tests were performed for each construct configuration using a calibrated mechanical load frame (Instron E3000, Norwood, MA) and calibrated 1 kN load cell (Instron Dynacell, Norwood, MA). Compression bending was selected as the loading mode because it was the failure mechanism identified in our previous retrieval study and replicates flexion motion [77]. A displacement-controlled rate of 25 mm/min compression was applied until a total displacement of 50 mm was reached. Six samples for each configuration were tested in ambient conditions for a total of 36 static compression bending samples. Load and displacement data were captured throughout the test and used to calculate stiffness, yield load, and peak load according to ASTM F1717 (MATLAB, MathWorks, Natick, MA) [38].

Dynamic Testing

Dynamic compression bending tests were also performed for each construct configuration using the same mechanical load frame and load cell. A load-controlled test was performed at 4 Hz between 150 N and 15 N compressive loads ($R = 0.1$) per a sinusoidal waveform until rod fracture occurred. Eight samples for each configuration were tested in ambient conditions for a total of 48 dynamic compression bending samples. The system software was programmed to monitor maximum and minimum displacements as well as changes in peak and valley load readings to detect rod fracture. Cycles to failure and failure location were recorded. Displacements were retrieved from the dataset at the following cycles to determine

how flexibility of the construct changed over time: 5,000 cycles, 50,000 cycles, and 1,000 cycles before failure. At each of these time points, the change in displacement was calculated by subtracting the displacements reached at the maximum and minimum loads. A digital optical microscope (Hirox-USA KH-7700, Hackensack, NJ) and scanning electron microscope (SEM, JEOL USA JSM-6390LV) were used to confirm the location of fracture initiation as described previously (Chapter 2).

Statistical Analysis

An analysis of variance (ANOVA) was used to assess statistical differences in mechanical properties between construct configurations at a significance level of $p \leq 0.05$ (Minitab Statistical Software, State College, PA). If the overall ANOVA showed significance, pairwise post-hoc comparisons were executed using Fisher's Least Significant Difference method and 95% confidence.

Results

Static Testing

All constructs experienced permanent deformation of the rods when loaded statically. A representative load-displacement curve with calculated mechanical parameters is shown in Figure 18, and Table 8 summarizes the mechanical parameters for all construct configurations. For the constructs with axial connectors present, the configurations with side-by-side connectors exhibited the lowest stiffness values and yield and peak loads. Additionally, yield and peak load for these constructs was similar to that from the no connector (rods only) construct group ($p > 0.4$). All

mechanical parameters (stiffness, yield load, peak load) significantly increased when the axial connector was changed from a side-by-side connector to a tandem connector. For configurations with tandem connectors, the results indicated greater stiffness, yield load, and peak load as the tandem connector length increased from 40 to 80 mm ($p < 0.001$).

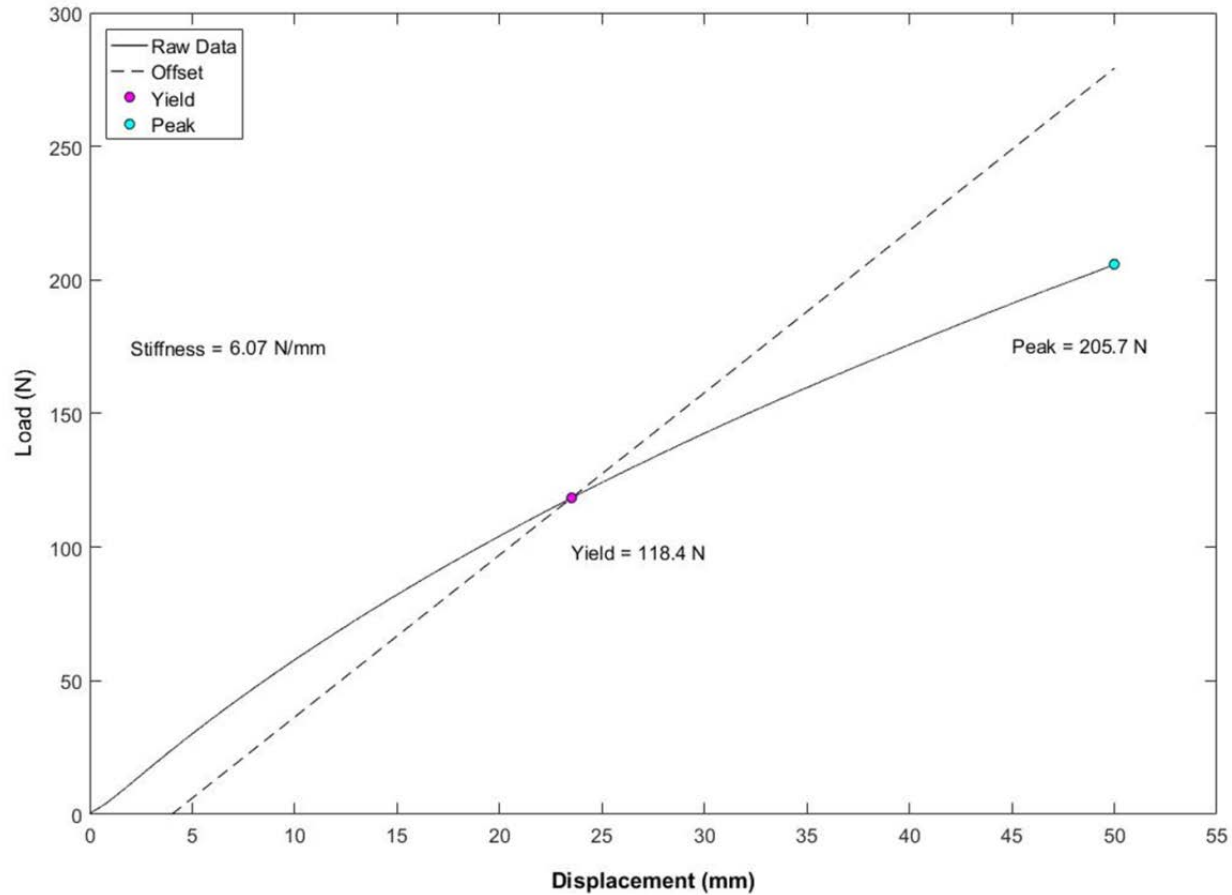


Figure 18: Sample load-displacement curve derived from MATLAB software for static compression bending tests. Stiffness was calculated using the 2% offset method. Yield load (pink circle) was the point where the offset (dashed line) intersected the curve (solid line). Peak load (blue circle) was based on the maximum load achieved at 50 mm total displacement.

Construct Configuration	Stiffness (N/mm)	Yield Load (N)	Peak Load (N)
	Mean \pm St. Deviation	Mean \pm St. Deviation	Mean \pm St. Deviation
No Connectors- Rods Only	5.8 ± 0.1^1	122.4 ± 2.8^A	$207.7 \pm 2.2^*$
Side-By-Side Connectors	Without crosslinks	6.0 ± 0.1^2	120.3 ± 3.1^A
	With crosslinks	5.6 ± 0.1^3	121.6 ± 2.6^A
40 mm Tandem Connectors	6.8 ± 0.1^4	153.1 ± 4.1^B	$247.6 \pm 1.7^\#$
80mm Tandem Connectors	Without crosslinks	8.8 ± 0.1^5	$309.4 \pm 3.3^\Sigma$
	With crosslinks	9.4 ± 0.2^6	$314.8 \pm 2.3^+$

Table 8: Results of Static Compression Bending Tests. Means in each column that do not share a letter, symbol, or number are significantly different.

The effect of adding crosslinks to the constructs was variable. The configuration containing an 80 mm tandem connector with crosslinks had a significantly higher stiffness than the 80 mm tandem connector configuration without crosslinks ($p < 0.001$). However, the side-by-side connector with crosslinks configuration had a significantly lower stiffness than the side-by-side connector configuration without crosslinks ($p < 0.001$). Yield load was not significantly affected by the addition of crosslinks for either the 80 mm tandem or side-by-side connector groups ($p > 0.1$).

Dynamic Testing

All dynamic constructs failed due to rod fracture, with fractures initiating on the posterior side of the rod. The fatigue results are displayed in Figure 19. The results showed that construct configurations with an axial connector alone (side-by-side, 40 mm tandem, and 80 mm tandem) had similar cycles to failure ($p > 0.07$). Interestingly, the cycles to failure for the construct configuration without connectors (rods only) was significantly different than that of the 40mm tandem connector configuration only ($p = 0.002$). The two construct configurations with crosslinks failed significantly earlier than their corresponding counterparts without crosslinks ($p < 0.015$). All four construct configurations without crosslinks experienced rod fracture adjacent to the pedicle screw while both construct configurations with crosslinks experienced rod fracture adjacent to the crosslink (Figure 20).

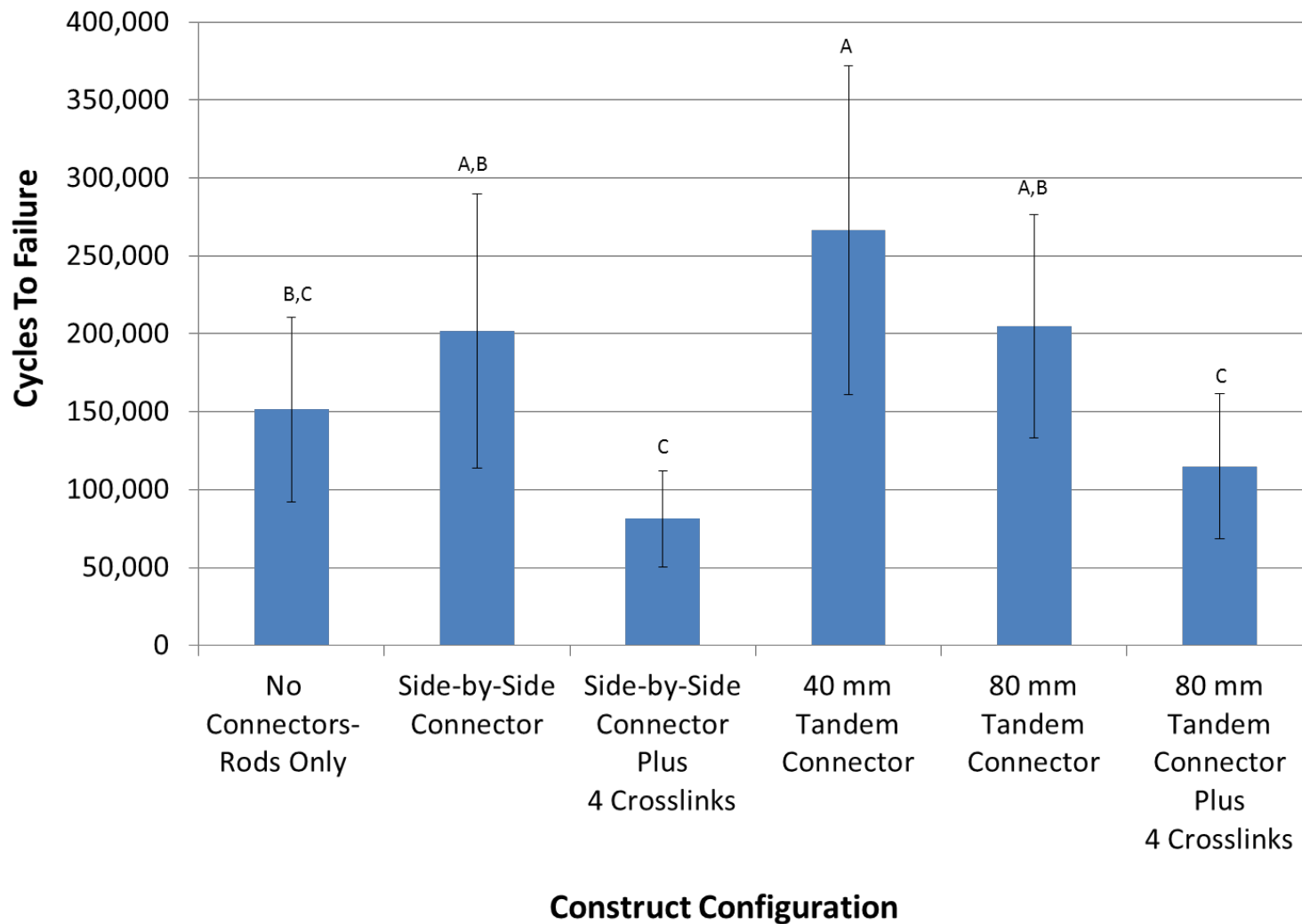


Figure 19: Fatigue performance for each construct configuration was captured through the number of cycles to failure during dynamic testing. All constructs were tested until rod fracture. Groups that do not share a letter are significantly different. Crosslinks significantly decreased the fatigue life of the constructs. Side-by-side and tandem connectors, regardless of length, have similar fatigue lives.

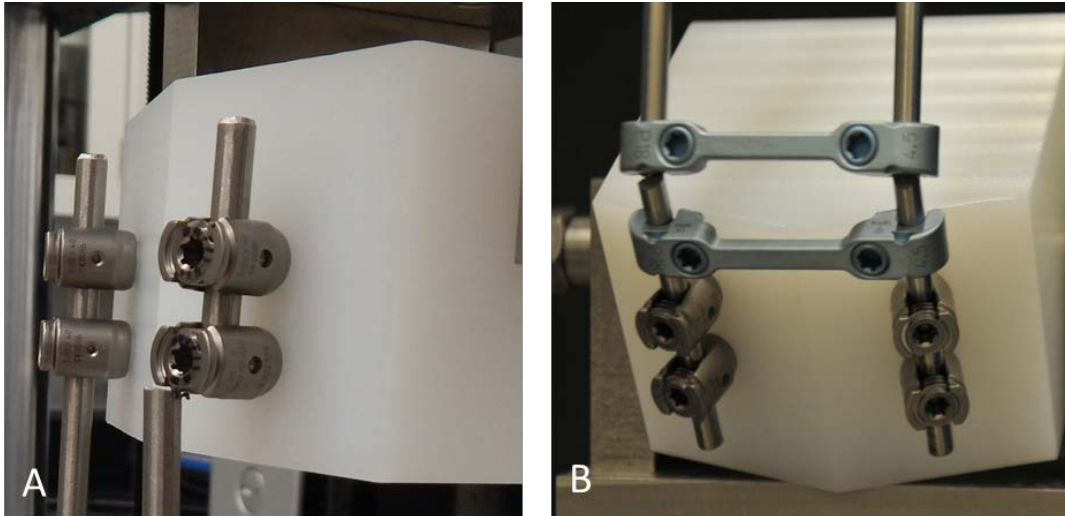


Figure 20: Examples of rod fracture after fatigue testing. The rods fractured adjacent to the pedicle screw (A) in four construct configurations. The remaining two construct configurations had crosslinks, and the location of rod fractures shifted adjacent to the crosslink (B). In all cases, fractures initiated on the posterior side of the rod adjacent to a stress concentration caused by either the pedicle screws or crosslinks.

The displacements during fatigue cycling varied based on the axial connector (Figure 21). All three of the construct configurations with tandem connectors (40 or 80 mm) experienced significantly lower displacements ($p < 0.001$) during fatigue testing at all time points as compared to groups that lacked a tandem connector (i.e., no connectors, side-by-side connectors with or without crosslinks). The two constructs with 80 mm tandem connectors exhibited significantly lower displacements than those present in configurations with 40mm tandem connectors ($p < 0.01$) and showed the lowest amount of displacement during fatigue testing overall. In general, the addition of crosslinks to the construct configuration did not alter the fatigue displacement as compared to its counterpart without crosslinks.

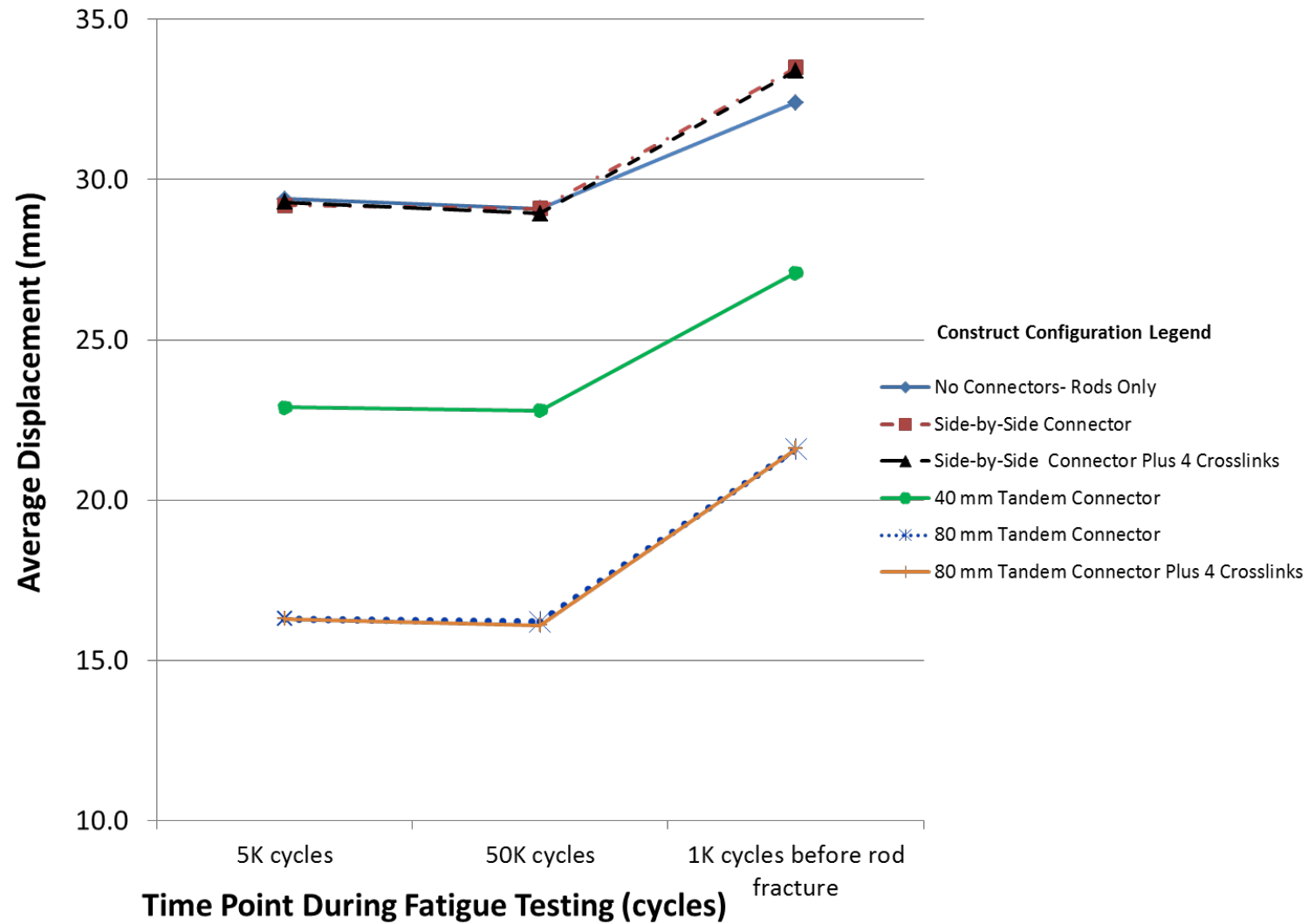


Figure 21: Graph showing displacement over time during fatigue testing. Displacement correlated to the type of axial connector, and the construct configurations with 80 mm tandem connectors (orange plus sign and blue star) allowed for the least amount of displacement. The groups with crosslinks (black triangle and orange plus sign) had similar displacements compared to their corresponding groups without crosslinks (red square and blue star, respectively).

Discussion

Traditional, distraction-based growing rod constructs have numerous possibilities of construct configurations since there are various types and lengths of connectors that can be chosen to achieve construct lengthening and rigidity [3]. Construct complexity is based primarily on surgeon preference and patient anatomy, and there has not been a systematic investigation of how various construct configurations may be linked to device failure. For example, it is important to understand the difference in mechanical performance of tandem versus side-by-side connectors because the distribution of stress within the construct may change depending on the type of axial connector selected. In addition, a mechanical bench model that can successfully simulate clinically-relevant scenarios in order to assess device performance and elucidate differences in construct configuration has not been developed. Therefore, the current study was designed to use a relevant non-clinical model for traditional, distraction-based growing rod constructs that can evaluate mechanical performance of various construct configurations.

The mechanical bench model developed herein successfully reproduced key findings from our previous growing rod retrieval study [77]. First, the model replicated fatigue fracture of the rod by imposing dynamic compression bending (by applying a bending moment through an offset axial load) to simulate flexion motion. Second, the location of rod fracture for the *in vitro* samples initiated on the posterior side of the rod, which is the same fracture initiation site as the *ex-vivo* samples. Third, *in vitro* tested samples fractured adjacent to stress concentrations caused by interconnecting components (e.g., set screws, crosslinks), which is consistent with our

previous retrieval study that revealed 62.5% of rod fractures initiated at a stress concentration [77]. These results suggest that the mechanical bench model used in this study is clinically relevant and may be the basis for assessing the mechanical performance of growing rod construct designs.

The current study identified important differences in mechanical performance of various growing rod construct configurations using the experimental model. Based on our prior retrieval study, we hypothesized that rigidity and lack of flexibility of the constructs were contributing to rod fracture [77]. This hypothesis was supported by the current study where we found that construct rigidity (reported as stiffness) and flexibility (reported as displacement) correlated with the types and lengths of the axial connector. In other words, the construct with the longest tandem connector of 80 mm and crosslinks was found to be the most rigid (highest stiffness from static testing) and least flexible (lowest displacement during fatigue testing). Moreover, the bench study demonstrated that crosslinks significantly decreased the fatigue performance of constructs compared to constructs without crosslinks. Crosslinks also shifted the location of fracture during dynamic testing to the local vicinity of the rod adjacent to the crosslink (Figure 20). The more interconnecting components present in the construct may also correspond to increased probability for fracture initiation given that additional stress concentrations are created on the posterior side of the rod. Therefore, the current bench study confirmed that constructs with tandem connectors and multiple crosslinks have decreased mechanical performance, which supports our hypothesis that the mechanical bench model can distinguish between stronger and weaker constructs by showing quantitatively significant differences in mechanical

performance (e.g., yield loads, stiffness values, and fatigue limits) between the configurations linked to failure compared to the configurations not linked to failure.

This study revealed the importance of evaluating both static and dynamic test results when evaluating device performance. For example, static testing showed that the 80 mm tandem connector with crosslinks configuration had the highest yield load, peak load, and stiffness (Table 8). Therefore, initially it would be reasonable to assume that this construct configuration is superior in terms of mechanical performance. However, the dynamic test results demonstrated that the fatigue performance for the configuration with 80 mm tandem connectors and crosslinks is significantly lower compared to the construct configurations without crosslinks (Figure 19). As another example, the static testing did not provide pertinent results about the flexibility of the construct, but the dynamic testing demonstrated that construct flexibility (displacement) changed throughout the test and varied based on the length of the axial connector (Figure 21). It is noted that dynamic results showed variability in cycles to failure within a test group, which is a limitation to this type of testing; however, we attempted to mitigate this limitation by increasing the sample size in each group. Although mechanical models are useful for replicating *in vivo* loading conditions in controlled environments, it is important to note that non-clinical models such as the one described in the current research study are limited in their ability to accurately reflect all conditions experienced by the device (e.g., patient factors).

A deformed, growing spine experiences multi-directional loading while the implants are keeping the spine distracted to help prevent progression of a scoliotic

curve and accommodate growth [1-3, 85]. Therefore, it may be more biomechanically favorable to use implants that are less rigid and allow more flexibility as opposed to resisting the motion of the spine. This concept was proposed by Yamaguchi et al.; however, bench studies were not performed to support this hypothesis [35]. The current study results combined with those of the previous retrieval study help support this concept that rigid and less flexible constructs (i.e., higher stiffness and lower displacement) demonstrate decreased mechanical performance.

Several recommendations were formulated based on the results of the current research study when considered in conjunction with our prior retrieval study [77]. We recommend that surgeons consider the number of interconnecting components used in the high stress regions of a pediatric growing rod construct, i.e., loaded area/active length. Both the retrieval and bench studies showed that the more interconnecting components included in the construct increases the rigidity and decreases the flexibility of the system, which are correlated with earlier failure. Additionally, more interconnecting components included in the construct also increases the number of stress concentrations along the weakest side of the rod (posterior) during the primary motion of flexion. Since fracture initiated on the posterior side in all retrievals and *in vitro* samples, it is important to minimize the stress along that side of the rod to help reduce the rod's susceptibility to fracture. We further recommend that crosslinks be implanted in low stress regions of the construct (outside of the anchor foundations). During the radiographic analysis in the retrieval study (Chapter 2), it was determined that all crosslinks were placed in the high stress regions of the construct (i.e., between the anchor foundations). Additionally, in this study, we further showed that crosslinks

were associated with earlier fatigue failure than the same construct configuration without crosslinks. Therefore, shifting the location of the crosslinks would allow for an increase in torsional rigidity without affecting bending fatigue performance by reducing the stress concentration on the rod caused by the interconnecting component. Serhan et al. verified that torsional stiffness could be achieved while still maintaining bending fatigue performance when the crosslinks are placed outside of the pedicle screws in the low stress region of the construct [70]. These recommendations along with those made in our prior retrieval study may help reduce the incidence of rod fracture and subsequent unplanned surgeries for patients with traditional, distraction-based growing rod constructs.

Chapter 5: Investigation of Growing Rod Lengthening using the Mechanical Bench Model

Introduction

Traditional, distraction-based growing rod constructs are an important contribution to the treatment of spinal deformities of young children [3, , 20, 39-42]. Lengthenings are a distinctive characteristic of these constructs used in children with early onset scoliosis (EOS) [11]. In order for the patient to reach their maximum growth potential and minimize cardiopulmonary complications, it is critical to avoid fusion and multi-level fixation of the implants [3]. Growing rods have the advantage of allowing for serial lengthenings across a non-fused spine to arrest curve progression [28]. Accordingly, patients undergo multiple surgical procedures throughout their treatment course, with a distraction-based lengthening occurring approximately every 6 to 12 months [28]. Growing rod constructs include axial connectors (side-by-side or tandem connector) where additional rod length is available for future distractions to avoid replacing the rod at each procedure. During a lengthening procedure, the axial connectors are loosened at the set screws, additional rod length is exposed so that the construct is distracted, and the connectors' set screws are tightened to lock the construct. As a result of manual lengthening of the construct, indentations occur on the rod in locations where the connectors' set screws previously interfaced with the rod. Existing rods are removed and replaced with new rods only in cases where the existing rods have fractured or are not long enough to extend further.

Despite the advantages of traditional, distraction-based growing rod constructs, these devices suffer from high complication rates including rod fracture [23, 30-34, 44, 45]. Since lengthenings are a unique feature of growing rod constructs, it is necessary to investigate how lengthenings impact their mechanical performance. Our prior retrieval study concluded that there was an increase in rod fracture with more lengthening procedures [77]. Constructs that were lengthened up to thirteen times over the course of treatment experienced significantly more rod fractures (3.6 ± 1.8 fractures) than constructs that were lengthened no more than four times (1.0 ± 0.0 fractures). Additionally, the retrieval study reported that 62.5% of failed rods fractured at a stress concentration, likely from indentations caused by the set screws of the axial connector. Other prior studies reported 4 to 6 lengthenings to be statistically associated with rod fracture [33, 34]. In contrast, Hosseini et al. reported no correlation between the number of lengthenings when comparing patients with and without rod fracture [71].

Lindsey et al., Dick et al., and Nguyen et al. have previously demonstrated that spinal rods made of common materials such as titanium (commercially pure or Ti6Al4V alloy), stainless steel 316L, or cobalt chromium alloy (CoCrMo) showed a significant decrease in fatigue performance when subjected to notching or indentations [74-76]. However, these studies concentrated on surgical techniques such as rod bending and they did not focus on techniques that are unique to growing rods such as lengthening. From these prior studies, it remains unclear whether rod fractures occurred because of lengthening alone, exposure of indentations alone, or a combination of both. Therefore, it is important to test for the effect of both

lengthening and exposure of indentations from interconnecting components in growing rod constructs.

The overall objective of the current research was to investigate the effect of lengthening on the mechanical performance of growing rod constructs. Consequently, three primary factors were explored under this objective: (1) impact of increased length of the construct in the absence of exposed indentations cause by the connectors' set screws, (2) impact of exposed indentations where the connectors' set screws previously interfaced with the rod in the absence of lengthening, and (3) the combination of increased construct length and exposed indentations. We hypothesize that the mechanical bench model can distinguish between the static and fatigue performance of constructs configured with different lengths and indentation exposures as described above by showing quantitatively significant differences in mechanical performance (e.g., yield loads, stiffness values, and fatigue limits). The current research can help us understand how lengthening impacts growing rod construct mechanical performance, which may aid in refining surgical techniques to help reduce rod fracture rates.

Methods

The first phase of the study examined the effects of lengthening on growing rod constructs, without exposing indentations where the connectors' set screws previously interfaced with the rod. The second phase of the study allowed for investigation of the effects of inducing indentations on growing rod constructs in the absence of construct lengthening. The third phase examined the effects of lengthening

on growing rod constructs while exposing the indentations by performing serial lengthening on the construct.

The mechanical bench model from Chapter 3 was used across the three phases of the study to address the overall objective. The test setup was based on ASTM F1717- *Standard Test Methods for Spinal Implant Constructs in a Vertebrectomy Model*, with deviations, fixturing, and construct configuration as described previously such that the test setup could accommodate a growing rod construct. A representative photograph of the test setup is displayed in Figure 22 showing that 80 mm tandem connectors were used and placed in the center of the construct. All set screws were torqued to 60in-lbs using a pre-set torque wrench. All components were made from Titanium alloy (Ti6Al4V) per ASTM F136 [84]. Compression bending was selected as the loading mode because it was the failure mechanism identified in our previous retrieval study and replicates flexion motion by applying a bending moment through an offset axial load [77].

Phase I: Effect of Construct Lengthening

Specimens underwent static compression bending testing using a calibrated mechanical load frame (Instron E3000, Norwood, MA) and calibrated 1 kN load cell (Instron Dynacell, Norwood, MA). A displacement-controlled rate of 25 mm/min compression was applied until a total displacement of 50 mm was reached. Load and displacement data were captured throughout the test and used to calculate stiffness, yield load, and peak load according to ASTM F1717 (MATLAB, MathWorks, Natick, MA) [38]. New specimens were then subjected to dynamic compression

bending testing using the same mechanical load frame and load cell. A load-controlled test was performed at 4Hz between 150N and 15N compressive loads ($R = 0.1$) per a sinusoidal waveform until rod fracture occurred. The system software was programmed to monitor peak and valley loads and displacements to detect rod fracture. Cycles to failure and failure location were recorded.

Two test groups were compared in this phase: the L_0 group represents the index length of the construct and the L_5 group represents the length of a construct after five lengthenings. Five lengthenings was chosen because it aligned with the number of lengthenings (four to six) that were described in previous studies as being statistically associated with rod fracture [33, 34]. The initial active length for the *in vitro* specimens (L_0) was determined to be 200mm based on average rod lengths from our prior retrieval study. The active length for L_5 was based a prior study by Noordeen et al. where the amount of distraction achieved during each lengthening surgery was reported [86]; therefore, the active length for L_5 was chosen as 255mm given this was the amount of distraction reported for the fifth lengthening. The L_0 and L_5 cohorts maintained their respective active lengths throughout the static and dynamic tests and, therefore, these groups did not have any exposed indentations from the connectors' set screws (Table 9). Six specimens were tested in each group for static testing and eight specimens were tested in each group for dynamic testing under ambient conditions.

Phase II: Effect of Indentations

The modified ASTM F1717 construct test was also utilized in this phase along with the same mechanical load frame and load cell. Dynamic compression bending testing was performed on the specimens until rod fracture using the identical setup and parameters outlined in Phase I above. Constructs in this phase (L_{indent}) were constructed with a constant 255mm active length and included pre-formed indentations from the axial connectors' set screws along the rod. Indentations were created at the same distances of distraction as in Phase III below and outlined in Table 9; however, all indentations were made prior to any fatigue testing so that construct lengthening was eliminated as a variable. Eight specimens were tested in this group under ambient conditions.

Phase III: Effect of Serial Lengthening

The modified ASTM F1717 construct test was also utilized in this phase along with the same mechanical load frame and load cell. Dynamic compression bending testing was performed on the specimens until rod fracture using the identical setup and parameters outlined in Phase I above. Constructs in this phase (L_{serial}) underwent serial lengthening procedures where both construct length and exposed indentations were simultaneously evaluated. More specifically, the L_{serial} specimens were distracted during the test to the lengthening distance (active length) outlined in Table 9 every 50,000 cycles to expose the prior indentations caused by the axial connectors' set screws. Each lengthening was performed by loosening the proximal end of the tandem connectors, distracting the rods to half the lengthening distance, tightening

the proximal set screws, and then performing the same steps at the distal end in order to reach the full lengthening distance. This group was limited to five lengthenings given the finite amount of additional rod housed within the 80mm tandem connector and for consistency with constructs in the L_5 group. If an L_{serial} construct reached a fifth and final lengthening without failure, the constructs remained at that length and were fatigued until rod fracture. Eight specimens were tested in this group under ambient conditions.

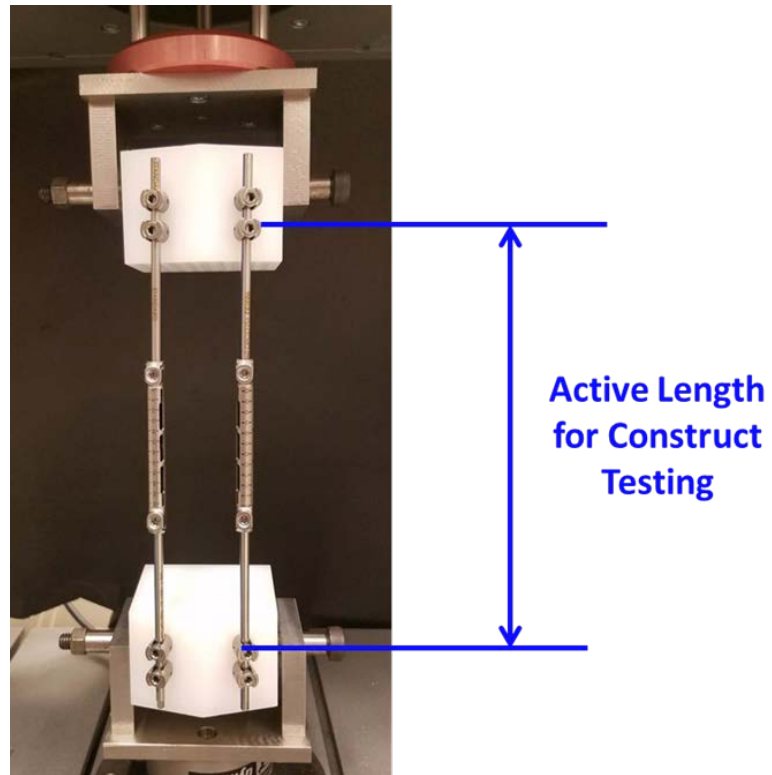


Figure 22: The test setup is based on ASTM F1717, modified to accommodate a pediatric growing rod construct. The active length of the construct was different for the groups described in Phases I-III.

Phase	Test Group	Active Length of the <i>in vitro</i> Test Construct		Indentations on the Rod?
I	Index Length (L_0)	200mm*		No
	Fifth Lengthening (L_5)	$L_0 + 55\text{mm} = 255\text{mm}^*$		No
II	Indentations (L_{indent})	255mm*		Yes, all indentations were created prior to testing at the same distances as L_{serial} group
III	Serial Lengthening (L_{serial})	Lengthening	Lengthening Distance*	Yes, exposed every 50,000 cycles per the lengthening schedule
		Index (L_0)	200 mm	
		1 st	200 mm + 17 mm = 217 mm	
		2 nd	217 mm + 10 mm = 227 mm	
		3 rd	227 mm + 11 mm = 238 mm	
		4 th	238 mm + 9 mm = 247 mm	
		5 th (L_5)	247 mm + 8 mm = 255 mm	

*Active lengths were derived from prior studies [77, 86]

Table 9: Construct Groups

Statistical Analysis

A two sample t-test was used to assess statistical differences in mechanical parameters at a significance level of $p \leq 0.05$. All statistical analyses were performed using Minitab® (Minitab Statistical Software, State College, PA).

Results

Phase I: Effect of Construct Lengthening

All static constructs experienced permanent deformation of the rods. The static test results are reported in Table 10. Constructs in the fully lengthened group (i.e., L₅) had significantly lower stiffness, yield load, and peak load than those in the index length group (i.e., L₀, $p < 0.001$). All constructs failed during dynamic testing due to rod fracture. The cycles to failure for each specimen in each test group are presented in Figure 23. The L₀ group had an average of $205,071 \pm 71,604$ cycles (range: 143,994 to 350,141 cycles), and the L₅ group had an average of $270,021 \pm 91,778$ cycles (range: 156,222 to 445,845 cycles). Constructs in the L₀ and L₅ groups had similar fatigue performance in terms of cycles to failure ($p = 0.19$) and experienced rod fracture adjacent to the pedicle screws.

Phase I Test Group	Stiffness (N/mm) Mean \pm St. Deviation	Yield Load (N) Mean \pm St. Deviation	Peak Load (N) Mean \pm St. Deviation
Index Length (L₀)	8.8 \pm 0.1	200.6 \pm 6.3	309.4 \pm 3.3
Fifth Lengthening (L₅)	6.3 \pm 0.3	141.9 \pm 4.7	218.5 \pm 1.8

Table 10: Results of Static Compression Bending Tests for Phase I Study.

Phase II: Effect of Indentations

Constructs in the L_{indent} group averaged 187,684 \pm 5 cycles (range: 123,403 to 276,351 cycles) until rod fracture. The cycles to failure for each specimen are presented in Figure 23. The cycles to failure for this group were similar to the cycles to failure for the L₅ group with the same active length of 255mm (p = 0.051). The rods in the L_{indent} group fractured adjacent to a pedicle screw and did not fracture in the vicinity of an exposed indentation made by the tandem connectors' set screws.

Phase III: Effect of Serial Lengthening

Constructs in the L_{serial} group reached a median active length of 238mm (or 3 lengthenings) before rod fracture, and therefore, could not be distracted to the full potential of 255mm (or 5 lengthenings). The cycles to failure for each specimen are also presented in Figure 23. The rods in the L_{serial} group fractured either adjacent to an

exposed indentation caused by the tandem connectors' set screws in 5/8 samples (Figure 24) or adjacent to a pedicle screw in 3/8 samples.

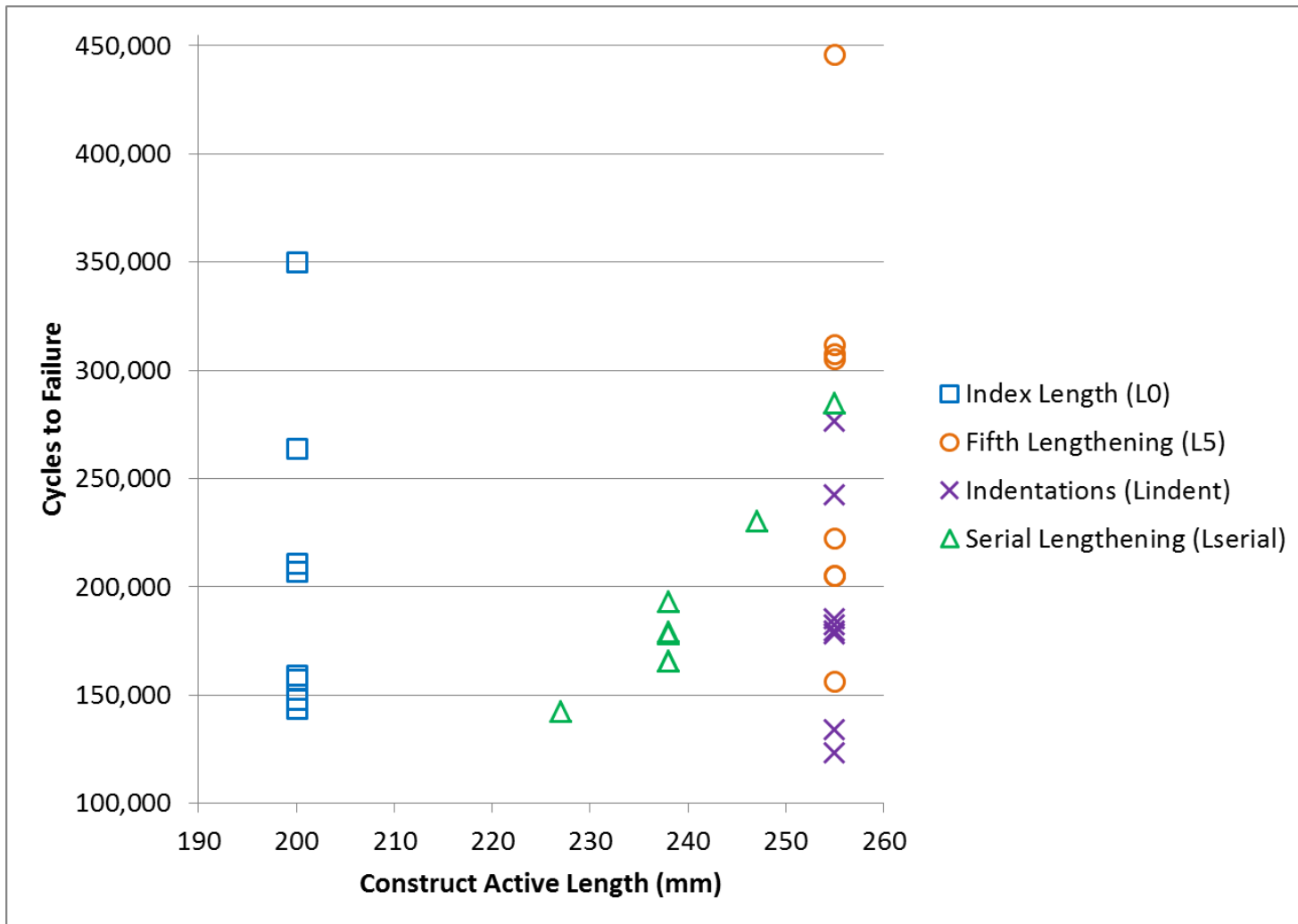


Figure 23: Results from dynamic compression bending. The index length group (blue square) has a 200mm active length based on rod lengths from our prior retrieval study. The fifth lengthening group (orange circle) has a 255mm active length and was included to evaluate lengthening alone without exposing indentations. The indentations group (purple X) has a 255mm active length and was included to evaluate indentations alone without lengthening. The serial lengthening group (green triangle) has an active length that changed every 50,000 cycles where indentations were exposed after each lengthening.

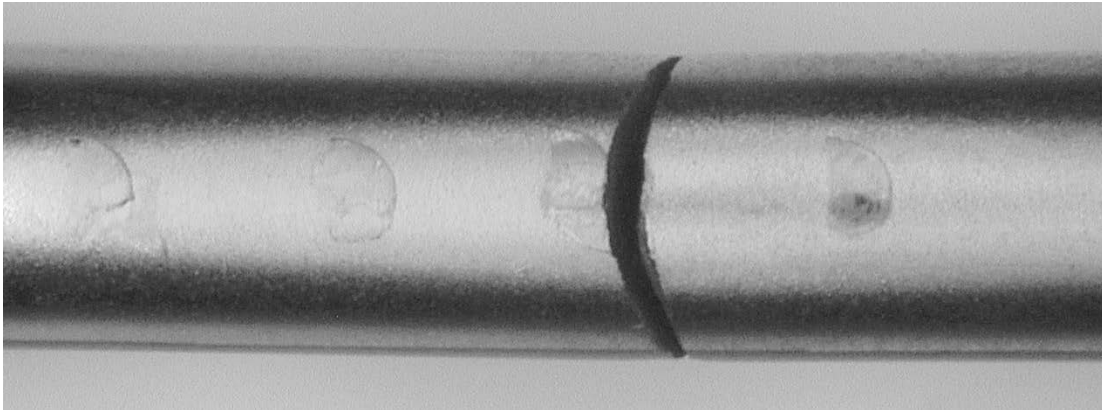


Figure 24: Photographs of an *in vitro* rod sample where the rod is lengthened to expose indentations made by set screws from the tandem connector. Rod fracture occurred in this location in 62.5% of samples in Phase III.

Discussion

The current research evaluated challenges associated with traditional, distraction-based growing rod constructs with the goal of understanding high complication rates [23, 30-34, 44, 45]. Specifically, this study was geared towards that goal by examining the interaction of mechanical performance with lengthening features such as increased construct length and exposure of prior indentations from interconnecting components. We were able to distinguish between lengthening alone, exposing indentations alone, and the combination of both to determine which variables have the greater effects on pediatric growing rod constructs.

When evaluating the results from Phase I, it can be concluded that construct lengthening alone does not significantly impact overall device performance, especially as it relates to fatigue performance. The static results showed that the 5th lengthening (L₅) group had lower yield load and stiffness compared to the index

length (L_0) group; however, these groups had similar fatigue performance, which is more representative of their clinical use. Additionally, the constructs in the L_0 and L_5 groups experienced rod fracture in the same locations during bench testing, i.e., adjacent to the pedicle screw. These results continued to show the importance of examining both static and dynamic results when making conclusions about device performance.

When evaluating the contribution of indentations alone (Phase II), this group showed that inducing indentations on the rod prior to applying mechanical stress on the construct does not have a significant impact on device performance. All rods in the L_{indent} group fractured adjacent to the pedicle screw and not at the indentations made prior to fatigue testing. This finding was consistent with results from the retrieval study where rods that experienced noticeable damage caused by surgical tools fractured in fatigue but at sites removed from tool damage. Additionally, the rods in the L_{indent} group had similar fatigue performance compared to the L_5 rods in Phase I that had the same active length.

The results for the L_{serial} group revealed that multiple exposed indentations greatly limit the number of lengthenings the construct can undergo before experiencing rod fracture which decreases its mechanical performance (Phase III). Indentations from serial lengthening create stress concentrations in the spinal rod which increases the number of points along the rod that are susceptible to fracture initiation. This is supported by the various locations of rod fracture during fatigue testing in the L_{serial} group as compared to the single location of rod fracture in the L_0 , L_5 , and L_{indent} groups. Therefore, we surmised that it is necessary to fatigue the rod at

each lengthening interval in order to induce rod fracture adjacent to the axial connector. The set screw of the axial connector is likely causing a stress on the rod during cyclical testing leading to crack initiation at that localized site. Then, exposing that crack initiation site after lengthening while the rod is undergoing bending resulted in crack propagation followed by final rupture. In other words, the friction and micro-motion between the interconnecting components play important roles in the rod's susceptibility to fracture. Therefore, through dynamic testing of growing rod constructs, this research demonstrated that the combined effect of exposing indentations from the connectors' set screws while simultaneously trying to achieve multiple lengthenings on mechanical performance is substantial.

These data support our hypothesis that the mechanical bench model can distinguish between the static and fatigue performance of constructs configured with different lengths and indentation exposures by showing quantitatively significant differences in mechanical performance (e.g., yield loads, stiffness values, and fatigue limits). Recommendations regarding surgical technique can be drawn from the current research. Rods should be replaced after a few lengthening procedures since these rods would have incurred multiple exposed stress concentrations and subjecting them to more fatigue cycles will allow for crack propagation and fatigue failure earlier than if they were replaced. This recommendation is supported by the results of the serial lengthening group that experienced rod fracture before achieving the maximum lengthening potential (i.e., three lengthenings instead of five). It is also advised that surgeons be aware of indentations located on the posterior side of the rod, which is also the side of the rod where all rod fractures initiated.

Chapter 6: Summary and Future Work

Summary

Growing rod treatment for children with early onset scoliosis is associated with high rates of rod fracture, which often lead to unplanned reoperations for these young patients. This research included the first study to examine multiple, retrieved pediatric growing rod constructs from various sites to systematically investigate the failure mode and mechanism, which tell us how and why the devices failed. Using classic failure analysis techniques in this understudied area, we have revealed that rod fracture (failure mode) is due to bending fatigue (failure mechanism), and damage caused by interconnecting components plays an important role in rod fractures. Despite the three-dimensional loading of a deformed spine compounded by the intricacies of a growing patient, we discovered that rod fracture predominantly occurred during flexion motion as opposed to complex, combined motions (e.g., bending plus torsion). Thereby, these data supported our hypothesis that rod fracture due to bending fatigue would be the most common failure mode/mechanism, and that crack initiation sites would be located near an indentation on the rod (e.g., stress concentration). This discovery provided an important contribution to the scoliosis community because it greatly simplified the requirements for developing a mechanical bench model to replicate clinical failures.

We have successfully developed and validated two clinically-relevant mechanical bench models in a device area that has no published test methodologies. Both bench models induced rod fracture due to bending fatigue, with the primary model having the ability to evaluate the mechanical performance of the growing rod

construct as a whole while the secondary model focused on specific components. The primary, construct bench model was used to evaluate the effect of construct complexity on mechanical properties and fatigue behavior. This model was also used to address unanswered questions about unique characteristics of pediatric growing rod constructs such as the effect of distraction-based lengthenings on construct performance. We were able to determine the key factors that had greater effects on the mechanical performance of the device such as stiff, inflexible constructs consisting of tandem connectors and multiple crosslinks. Therefore, data derived from the mechanical testing studies supported our hypothesis that the mechanical bench model can distinguish between stronger and weaker constructs by showing quantitatively significant differences in mechanical performance between the configurations linked to failure compared to the configurations not linked to failure. The development, validation, and use of mechanical testing have offered significant contributions to the scientific community as researchers now have resources and tools to evaluate pediatric growing rod constructs and verify device improvements.

This research significantly impacts a small, yet important patient population. More specifically, key recommendations were made through the retrieval study that can lead to improvements in surgical technique and device design. If these recommendations are executed, they have the potential to impact the quality of life for patients that undergo numerous surgical procedures during their treatment period by reducing the incidence of rod fracture. These recommendations included the use of torque-limiting wrenches as well as frequent exchange of rods during scheduled surgeries in syndromic patients and in patients that experience prior rod fracture.

Additional recommendations were made and verified through a mechanical performance assessment using the proposed bench models. These included considering the number of interconnecting components used in the high stress regions of a pediatric growing rod construct, and the use of numerous interconnecting components that increases the rigidity and decreases the flexibility of the construct. Additionally, the more interconnecting components included in the construct increases the number of stress concentrations along the weakest side of the rod (posterior) during the primary motion of flexion.

We further recommended that crosslinks be implanted in low stress regions of the construct as this would allow for an increase in torsional rigidity without affecting bending fatigue performance. Rods should be replaced after several lengthening procedures since these rods incur multiple exposed stress concentrations where the likelihood that a crack was previously initiated was high. It is also advised that surgeons be aware of indentations located on the posterior side of the rod, which is also the side of the rod where all rod fractures initiated (during both the retrieval and bench studies). We explored the idea of rotating the stress concentrations away from the posterior side of the rod and saw a dramatic extension of the fatigue performance of the rod. All three rotated rods reached runout of 1 million cycles and, therefore, did not experience rod fracture (using the secondary bench model and methods outlined in Chapter 3). Future work is needed to thoroughly evaluate this idea and other ideas on reducing stress concentrations on the posterior side of the rod. Ultimately, the information revealed through the subject research can be used to reduce the number

of unplanned reoperations of growing rod patients, especially as it relates to rod fractures that may be preventable based on these recommendations.

Future Work

Children with severe scoliosis are part of a vulnerable population that is understudied so more work is needed to optimize current treatment strategies and develop new devices. The findings from this research can be applied towards various areas of future work. Some researchers have focused on eliminating the need for surgical lengthening procedures by investigating the use of magnetically-controlled growing rod constructs. The rods are lengthened through an external controller that communicates with a magnetic actuator within the rod. Therefore, the growing rod construct does not consist of axial connectors that require manual manipulation for lengthening. While this new technology has significant benefits for the patient in terms of reducing the number of surgeries, rod fracture is still documented with these devices [87, 88]. Therefore, future work is needed to replicate rod fracture in magnetically-controlled growing rod constructs with the established mechanical bench models to determine how to improve the construct's ability to resist failure. Regardless of the mechanism used to lengthen the construct, the magnetically-controlled devices would be subjected to similar bending fatigue loads as traditional growing rod construct and, therefore, can be tested using the same proposed mechanical bench models.

Computational modeling is another area for future work. Finite element analysis (FEA) of pediatric growing rod constructs would enable systematic investigation of multiple patient and device factors for their impact on device fracture

in a more efficient manner than experimental bench testing. We have initiated this work by developing computational models of the experimental bench tests based on ASTM F1717 device configurations in order to predict stress in the rod and fatigue failure. Additionally, we have validated these computational models using our experimental data acquired from multiple construct configurations and found that the computational model is able to predict the construct's mechanical behavior with high accuracy. This gives us confidence in the predicted stress distribution within the rod and construct, and the ability to address more unanswered questions about growing rod constructs. Through this computational model of the experimental bench test, we can more efficiently investigate device factors (e.g., rod material) for their effect on stress distribution and rod fracture. In addition, we have started developing models of growing rod constructs implanted into spinal anatomies based on patients identified in our retrieval study in order to investigate some of the interactions between anatomy (e.g., Cobb angle) and device features on rod fracture. However, future work is needed to fully utilize patient-specific models and perform simulations of growing rod constructs in the patient while undergoing relevant spinal motion.

Lastly, pediatric spinal devices need standardized test methodologies. Standards, such as those published through the American Society of Testing and Materials (ASTM International), are important contributions to the medical device community. The test methods within standards provide the opportunity for uniform testing across device generations and different device manufacturers. For example, consistent testing provides a direct comparison between first and second generation devices to determine if the second generation is indeed improved. Regulatory bodies

like the U.S. Food and Drug Administration rely heavily on standard test methods to determine whether new spinal implants are as safe and effective as implants already on the market, even if they are created by different manufacturers. The bench models established through this research can be used in the development of standard test methods since they are based on clinically-documented failures. Based on the findings of this dissertation, the following suggestions should be considered in the development of a standard test method for the construct mechanical bench model:

- We found that bending fatigue is the dominant loading condition to apply. It is simulated by applying a bending moment through an offset axial compressive load. Therefore, a modified version of ASTM F1717 is suggested. The proposed modifications in Figure 12 are suitable for the evaluation of pediatric growing rod constructs and account for the use of various components and construct configurations.
- Offset test blocks are suggested when using side-by-side connectors to keep rods parallel to the direction of the applied load (see Appendix 2).
- The torque used to tighten set screws should be consistent and recorded. A torque-limiting wrench should be used to prevent overload failure on the rod as revealed through the retrieval study.
- A load-controlled test allows for the minimum and maximum displacement values to be monitored throughout fatigue testing. The change in displacement during fatigue testing provides supportive information about the construct flexibility.

- Serial lengthening is recommended to simulate the clinical condition in growing rod constructs. The lengthening schedule used in this research was based on previous publication [86] and can be used as a guide, but may need to be adjusted based on the application.
- The sample should be fatigued until rod fracture occurs. This research demonstrated that rod fracture can be achieved in less than 500,000 cycles when the test is performed between compressive loads of 15N and 150N.
- The retrieval analysis revealed that fractures initiated on the posterior side of the rod. When replicating failures from the retrievals, the location of fracture initiation can be verified through microscopic evaluation.

Appendices

[Appendix 1: Retrieval analysis protocol](#)

[Appendix 2: Drawings of UHMWPE test blocks](#)

[Appendix 3: Standard operating procedures for mechanical testing](#)

Bibliography

1. Sangole, A.P., et al., *Three-dimensional classification of thoracic scoliotic curves*. Spine (Phila Pa 1976), 2009. 34(1): p. 91-9.
2. Stokes, I.A., L.C. Bigalow, and M.S. Moreland, *Measurement of axial rotation of vertebrae in scoliosis*. Spine (Phila Pa 1976), 1986. 11(3): p. 213-8.
3. Akbarnia, B.A., M. Yazici, and G.H. Thompson, *The growing spine: management of spinal disorders in young children*. 2010: Springer Science & Business Media.
4. Williams, B.A., et al., *Development and initial validation of the Classification of Early-Onset Scoliosis (C-EOS)*. JBJS, 2014. 96(16): p. 1359-1367.
5. Dimeglio, A., *Growth of the Spine Before Age 5 Years*. Journal of Pediatric Orthopaedics B, 1992. 1(2): p. 102-107.
6. Andersson, G., *The burden of musculoskeletal diseases in the United States: Prevalence, societal and economic cost*. 2008: Amer Academy of Orthopaedic.
7. Campbell, R.M. and M.D. Smith, *Thoracic insufficiency syndrome and exotic scoliosis*. J Bone Joint Surg Am, 2007. 89 Suppl 1: p. 108-22.
8. Pehrsson, K., et al., *Long-term follow-up of patients with untreated scoliosis. A study of mortality, causes of death, and symptoms*. Spine (Phila Pa 1976), 1992. 17(9): p. 1091-6.
9. Phillips, J.H., D.R. Knapp, and J. Herrera-Soto, *Mortality and morbidity in early-onset scoliosis surgery*. Spine (Phila Pa 1976), 2013. 38(4): p. 324-7.
10. Fu, K.M., et al., *Morbidity and mortality associated with spinal surgery in children: a review of the Scoliosis Research Society morbidity and mortality database*. J Neurosurg Pediatr, 2011. 7(1): p. 37-41.
11. Akbarnia, B.A., R.M. Campbell, and R.E. McCarthy, *Optimizing Safety and Outcomes in Spinal Deformity Surgery: Early-Onset Scoliosis*. Spine Deformity, 2012.
12. Cobb, J., *Outline for the study of scoliosis*. Instr Course Lect, 1948. 5: p. 261-275.
13. Anderson, A.L., et al., *The Effect of Posterior Thoracic Spine Anatomical Structures on Motion Segment Flexion Stiffness*. Spine, 2009. 34(5): p. 441-446.
14. Mehta, M.H., *Growth as a corrective force in the early treatment of progressive infantile scoliosis*. J Bone Joint Surg Br, 2005. 87(9): p. 1237-47.
15. Greiner, K.A., *Adolescent idiopathic scoliosis: radiologic decision-making*. Am Fam Physician, 2002. 65(9): p. 1817-22.
16. Lonstein, J.E. and J.M. Carlson, *The prediction of curve progression in untreated idiopathic scoliosis during growth*. J Bone Joint Surg Am, 1984. 66(7): p. 1061-71.
17. Dubousset, J., J.A. Herring, and H. Shufflebarger, *The crankshaft phenomenon*. J Pediatr Orthop, 1989. 9(5): p. 541-50.
18. ROGERS, S.P., *Mechanics of scoliosis*. Archives of Surgery, 1933. 26(6): p. 962-980.

19. HARRINGTON, P.R., *Treatment of scoliosis. Correction and internal fixation by spine instrumentation.* J Bone Joint Surg Am, 1962. 44-A: p. 591-610.
20. Fletcher, N.D., et al., *Current treatment preferences for early onset scoliosis: a survey of POSNA members.* J Pediatr Orthop, 2011. 31(3): p. 326-30.
21. Greggi, T., et al., *Complications incidence in the treatment of early onset scoliosis with growing spinal implants.* Stud Health Technol Inform, 2012. 176: p. 334-7.
22. Flynn, J.M., et al., *Growing-rod graduates: lessons learned from ninety-nine patients who completed lengthening.* J Bone Joint Surg Am, 2013. 95(19): p. 1745-50.
23. Farooq, N., et al., *Minimizing complications with single submuscular growing rods: a review of technique and results on 88 patients with minimum two-year follow-up.* Spine (Phila Pa 1976), 2010. 35(25): p. 2252-8.
24. Miladi, L., A. Journe, and M. Mousny, *H3S2 (3 hooks, 2 screws) construct: a simple growing rod technique for early onset scoliosis.* Eur Spine J, 2013. 22 Suppl 2: p. S96-105.
25. Elsebai, H.B., et al., *Safety and efficacy of growing rod technique for pediatric congenital spinal deformities.* J Pediatr Orthop, 2011. 31(1): p. 1-5.
26. Moe, J.H., et al., *Harrington instrumentation without fusion plus external orthotic support for the treatment of difficult curvature problems in young children.* Clin Orthop Relat Res, 1984(185): p. 35-45.
27. Mineiro, J. and S.L. Weinstein, *Subcutaneous rodding for progressive spinal curvatures: early results.* J Pediatr Orthop, 2002. 22(3): p. 290-5.
28. Akbarnia, B.A., et al., *Dual growing rod technique for the treatment of progressive early-onset scoliosis: a multicenter study.* Spine (Phila Pa 1976), 2005. 30(17 Suppl): p. S46-57.
29. Thompson, G.H., B.A. Akbarnia, and R.M. Campbell, *Growing rod techniques in early-onset scoliosis.* J Pediatr Orthop, 2007. 27(3): p. 354-61.
30. Sankar, W.N., D.C. Acevedo, and D.L. Skaggs, *Comparison of complications among growing spinal implants.* Spine (Phila Pa 1976), 2010. 35(23): p. 2091-6.
31. Bess, S., et al., *Complications of growing-rod treatment for early-onset scoliosis: analysis of one hundred and forty patients.* J Bone Joint Surg Am, 2010. 92(15): p. 2533-43.
32. Zebala, L.P., et al. *Dual Growing Rod Instrumentation with Pedicle Screw Foundation at a Single Institution: Assessment of Outcomes and Complications: E-Poster# 23.* in *Spine Journal Meeting Abstracts.* 2009. LWW.
33. Watanabe, K., et al., *Risk factors for complications associated with growing-rod surgery for early-onset scoliosis.* Spine (Phila Pa 1976), 2013. 38(8): p. E464-8.
34. Yang, J.S., et al., *Growing rod fractures: risk factors and opportunities for prevention.* Spine (Phila Pa 1976), 2011. 36(20): p. 1639-44.
35. Yamaguchi, K.T., et al., *Are rib versus spine anchors protective against breakage of growing rods?* Spine Deformity, 2014. 2(6): p. 489-492.

36. Yamanaka, K., et al., *Analysis of the Fracture Mechanism of Ti-6Al-4V Alloy Rods that failed Clinically after Spinal Instrumentation Surgery*. Spine, 2015.
37. International, A., *ASM Handbook: Volume 11: Failure Analysis and Prevention*. Vol. 11. 2002, Materials Park, Ohio: ASM International. 1164.
38. International, A., *ASTM F1717-15 "Standard Test Methods for Spinal Implant Constructs in a Vertebrectomy Model"*. 2015: West Conshohocken, PA.
39. Tis, J.E., et al., *Early onset scoliosis: modern treatment and results*. J Pediatr Orthop, 2012. 32(7): p. 647-57.
40. Vitale, M.G., et al., *Variability of expert opinion in treatment of early-onset scoliosis*. Clin Orthop Relat Res, 2011. 469(5): p. 1317-22.
41. Yang, J.S., et al., *Growing rods for spinal deformity: characterizing consensus and variation in current use*. Journal of Pediatric Orthopaedics, 2010. 30(3): p. 264-270.
42. Yazici, M. and Z.D. Olgun, *Growing rod concepts: state of the art*. Eur Spine J, 2013. 22 Suppl 2: p. S118-30.
43. Akbarnia, B.A., et al., *Dual growing rod technique followed for three to eleven years until final fusion: the effect of frequency of lengthening*. Spine (Phila Pa 1976), 2008. 33(9): p. 984-90.
44. Akbarnia, B.A. and J.B. Emans, *Complications of growth-sparing surgery in early onset scoliosis*. Spine (Phila Pa 1976), 2010. 35(25): p. 2193-204.
45. Wattenbarger, J.M., B.S. Richards, and J.A. Herring, *A comparison of single-rod instrumentation with double-rod instrumentation in adolescent idiopathic scoliosis*. Spine, 2000. 25(13): p. 1680-1688.
46. Akazawa, T., et al., *Corrosion of spinal implants retrieved from patients with scoliosis*. Journal of Orthopaedic Science, 2005. 10(2): p. 200-205.
47. Aulisa, L., et al., *Corrosion of the Harrington's instrumentation and biological behaviour of the rod-human spine system*. Biomaterials, 1982. 3(4): p. 246-IN1.
48. del Rio, J., J. Beguiristain, and J. Duarte, *Metal levels in corrosion of spinal implants*. European Spine Journal, 2007. 16(7): p. 1055-1061.
49. Kirkpatrick, J.S., et al., *Corrosion on spinal implants*. Journal of spinal disorders & techniques, 2005. 18(3): p. 247-251.
50. Majid, K., et al., *Analysis of in vivo corrosion of 316L stainless steel posterior thoracolumbar plate systems: a retrieval study*. Journal of spinal disorders & techniques, 2011. 24(8): p. 500-505.
51. Prikryl, M., et al., *Role of corrosion in Harrington and Luque rods failure*. Biomaterials, 1989. 10(2): p. 109-117.
52. Vieweg, U., et al., *Corrosion on an internal spinal fixator system*. Spine, 1999. 24(10): p. 946-951.
53. Villarraga, M.L., et al., *Wear and corrosion in retrieved thoracolumbar posterior internal fixation*. Spine, 2006. 31(21): p. 2454-2462.
54. Singh, V., et al., *Growth Guidance System for Early-Onset Scoliosis: Comparison of Experimental and Retrieval Wear*. Spine, 2013. 38(18): p. 1546-1553.

55. Bidez, M., et al., *Biodegradation Phenomena Observed in In Vivo and In Vitro Spinal Instrumentation Systems*. Spine, 1987. 12(6): p. 605-608.
56. Brunski, J., D. Hill, and A. Moskowitz, *Stresses in a Harrington distraction rod: Their origin and relationship to fatigue fractures in vivo*. Journal of biomechanical engineering, 1983. 105(2): p. 101-107.
57. Chen, C.-S., et al., *Failure analysis of broken pedicle screws on spinal instrumentation*. Medical engineering & physics, 2005. 27(6): p. 487-496.
58. Cundy, T.P., et al., *Chromium ion release from stainless steel pediatric scoliosis instrumentation*. Spine, 2010. 35(9): p. 967-974.
59. COOK, S.D., et al., *An analysis of failed Harrington rods*. Spine, 1985. 10(4): p. 313-316.
60. International, A., *ASTM Standard F561-13 "Standard Practice for Retrieval and Analysis of Medical Devices, and Associated Tissues and Fluids"*. 2013: West Conshohocken, PA.
61. Cidambi, K.R., et al., *Postoperative changes in spinal rod contour in adolescent idiopathic scoliosis: an in vivo deformation study*. Spine, 2012. 37(18): p. 1566-1572.
62. Schroerlucke, S.R., et al., *How does thoracic kyphosis affect patient outcomes in growing rod surgery?* Spine, 2012. 37(15): p. 1303-1309.
63. Agarwal, A., et al., *Smaller Interval Distractions May Reduce Chances of Growth Rod Breakage Without Impeding Desired Spinal Growth: A Finite Element Study*. Spine Deformity, 2014. 2(6): p. 430-436.
64. Melkerson, M.N., S.L. Griffith, and J.S. Kirkpatrick, *Spinal Implants: Are We Evaluating Them Appropriately?* Vol. 1431. 2003: Astm International.
65. Ashman, R.B., et al., *Mechanical testing of spinal instrumentation*. Clinical orthopaedics and related research, 1988. 227: p. 113-125.
66. Stambough, J.L., et al., *Effects of cross-linkage on fatigue life and failure modes of stainless steel posterior spinal constructs*. Journal of Spinal Disorders & Techniques, 1998. 11(3): p. 221-226.
67. Dick, J.C., et al., *Mechanical Evaluation of Cross-Link Designs in Rigid Pedicle Screw Systems*. Spine, 1997. 22(4): p. 370-375.
68. Lynn, G., et al., *Mechanical stability of thoracolumbar pedicle screw fixation: the effect of crosslinks*. Spine, 1997. 22(14): p. 1568-1572.
69. Kuklo, T.R., et al., *Biomechanical contribution of transverse connectors to segmental stability following long segment instrumentation with thoracic pedicle screws*. Spine, 2008. 33(15): p. E482-E487.
70. Serhan, H., Giorgio, P., Torres, K., and Slivka, M., *Spinal implant transverse rod connectors: A delicate balance between stability and fatigue performance*. ASTM Special Technical Publication, 2002. 1431: p. 34-39.
71. Hosseini, P., et al., *Rod fracture and lengthening intervals in traditional growing rods: is there a relationship?* European Spine Journal, 2016: p. 1-6.
72. Serhan, H., et al., *Would CoCr rods provide better correctional forces than stainless steel or titanium for rigid scoliosis curves?* Journal of spinal disorders & techniques, 2013. 26(2): p. E70-E74.

73. Slivka, M.A., Y.K. Fan, and J.C. Eck, *The Effect of Contouring on Fatigue Strength of Spinal Rods: Is it Okay to Re-bend and Which Materials Are Best?* Spine Deformity, 2013. 1(6): p. 395-400.
74. Dick, J.C. and C.A. Bourgeault, *Notch sensitivity of titanium alloy, commercially pure titanium, and stainless steel spinal implants.* Spine, 2001. 26(15): p. 1668-1672.
75. Nguyen, T.Q., et al., *The fatigue life of contoured cobalt chrome posterior spinal fusion rods.* Proc Inst Mech Eng H, 2011. 225(2): p. 194-8.
76. Lindsey, C., et al., *The effects of rod contouring on spinal construct fatigue strength.* Spine (Phila Pa 1976), 2006. 31(15): p. 1680-7.
77. Hill, G., et al., *Retrieval and clinical analysis of distraction-based dual growing rod constructs for early onset scoliosis.* The Spine Journal, 2017.
78. Niu, C., et al., *Reduction-fixation spinal system in spondylolisthesis.* American journal of orthopedics (Belle Mead, NJ), 1996. 25(6): p. 418-424.
79. Matsuzaki, H., et al., *Problems and solutions of pedicle screw plate fixation of lumbar spine.* Spine, 1990. 15(11): p. 1159-1165.
80. Dickman, C.A., et al., *Transpedicular screw-rod fixation of the lumbar spine: operative technique and outcome in 104 cases.* Journal of neurosurgery, 1992. 77(6): p. 860-870.
81. Hibbeler, R.C., *Mechanics of Materials.* 6th ed. 2016: Pearson Education.
82. Lee, C., K.S. Myung, and D.L. Skaggs, *Some Connectors in Distraction-based Growing Rods Fail More Than Others.* Spine Deformity. 1(2): p. 148-156.
83. Mahar, A.T., et al., *Biomechanical comparison of different anchors (foundations) for the pediatric dual growing rod technique.* Spine Journal, 2008. 8(6): p. 933-939.
84. International, A., *ASTM F136-13, Standard Specification for Wrought Titanium-6Aluminum-4Vanadium ELI (Extra Low Interstitial) Alloy for Surgical Implant Applications (UNS R56401).* 2013: West Conshohocken, PA.
85. Birchall, D., et al., *Demonstration of vertebral and disc mechanical torsion in adolescent idiopathic scoliosis using three-dimensional MR imaging.* European Spine Journal, 2005. 14(2): p. 123-129.
86. Noordeen, H.M., et al., *In vivo distraction force and length measurements of growing rods: which factors influence the ability to lengthen?* Spine (Phila Pa 1976), 2011. 36(26): p. 2299-303.
87. Hosseini, P., et al., *Magnetically controlled growing rods for early-onset scoliosis: a multicenter study of 23 cases with minimum 2 years follow-up.* Spine, 2016. 41(18): p. 1456-1462.
88. Keskinen, H., et al., *Preliminary comparison of primary and conversion surgery with magnetically controlled growing rods in children with early onset scoliosis.* European Spine Journal, 2016. 25(10): p. 3294-3300.